NASA TECHNICAL NOTE

NASA TN D-3787

NASA TN D-3787

A SYNOPTIC WORLD WEATHER ANALYSIS OF TIROS VII RADIATION DATA

by

Lewis J. Allison
Goddard Space Flight Center
Greenbelt, Md.

and

Guenter Warnecke
Freie Universität Berlin
Berlin, West Germany

NATIONAL AERONAUTICS AND SPACE ADMINISTRATION • WASHINGTON, D. C. • JUNE 1967

A SYNOPTIC WORLD WEATHER ANALYSIS OF TIROS VII RADIATION DATA

By Lewis J. Allison
Goddard Space Flight Center
Greenbelt, Md.

and

Guenter Warnecke
Freie Universität Berlin
Berlin, West Germany

NATIONAL AERONAUTICS AND SPACE ADMINISTRATION

For sale by the Clearinghouse for Federal Scientific and Technical Information
Springfield, Virginia 22151 – CFSTI price $3.00

ABSTRACT

A synoptic world weather analysis of TIROS VII radiation data was made for January 21-22, 1964. The distribution of quasi-global cloudiness inferred from the channel 2 (8-12μ) "atmospheric window" data was compared with a previously published, July 16, 1961, study of TIROS III 8-12μ radiation data. The January 1964 radiation-synoptic analysis is characterized by a small difference in outgoing radiation between the winter and summer hemispheres. It was also noted that mid-latitude frontal systems extend into the sub-tropics during the southern hemisphere summer. The January-July radiation study tends to confirm our premise that the 8-12μ infrared region is suited for global synoptic detection and tracking of meso-scale meteorological features.

CONTENTS

A SYNOPTIC WORLD WEATHER ANALYSIS OF TIROS VII RADIATION DATA

by
Lewis J. Allison
Goddard Space Flight Center

and

Guenter Warnecke
Freie Universität Berlin

INTRODUCTION

The TIROS series of radiation experiments has produced a large amount of synoptic information which is useful for analysis of the vertical and horizontal structure of the atmosphere. One of the major advantages of a satellite radiation measurement system is that it provides a nearly global mapping of certain meteorological parameters of the atmosphere on a regular basis. This study analyzes a quasi-global radiation map for January 21-22, 1964, and compares it with conventional world-wide synoptic weather observations and analyses. A seasonal comparison is made with a July 16, 1961 radiation study in order to compare the differences in outgoing radiation patterns in both hemispheres. The significance of derived meso-meteorological features and the climatological circulation patterns is discussed.

METHOD OF ANALYSIS

The January 21-22, 1964 date was selected because, fortunately, nine orbits of TIROS VII radiation data were recorded during this period. Since only 5 to 8 out of 14 possible orbits are normally acquired daily, these data provided the optimum in daily world radiation coverage in the northern hemisphere mid-winter season.

The subsatellite tracks of the nine orbital passes, 3195 through 3203, are shown in Figure 1. The solid and dashed lines indicate the single open and alternating open modes, respectively, along the subsatellite paths. (See Appendix B of Reference 1 for a discussion of the radiometer scanning modes.) The beginning and ending times of the scanning modes are shown in minutes with respect to the ascending node time at the equator. Since closed mode data did not occur during the period of study, major data mislocation problems were avoided. Although mislocations of single swaths in the alternating mode can occur, they should be of minor importance because of the data averaging

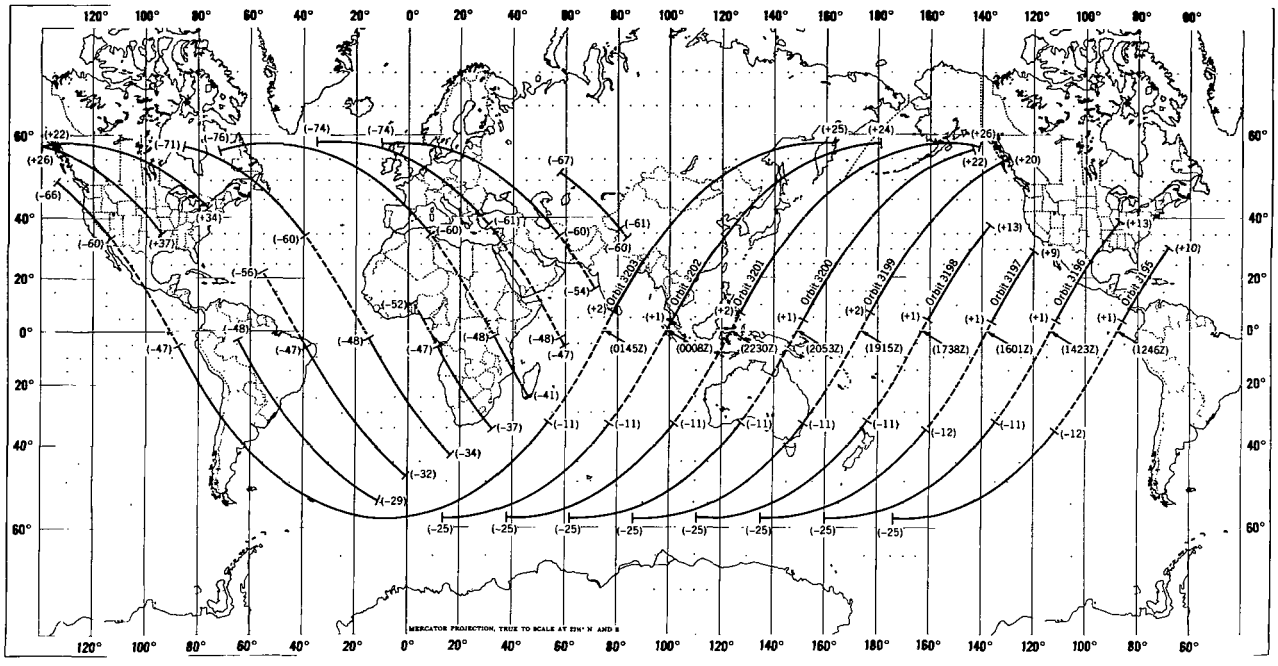

Figure 1—Pattern of the orbits of TIROS VII, on January 21-22, 1964 used for the quasi-global radiation map (Plate 1). The orbital numbers and the related ascending node times are drawn at the beginning of each orbit. The number along the orbital tracks are minutes from ascending node time.

procedures involved in the computer mapping program. The channel 2 data for the nine orbits were processed into 1:20 million scale mercator grid print maps by an IBM 7094 computer, using a resolution of 2.5 degrees of longitude per mesh interval and a scan nadir angle limitation of 60 degrees. The infrared data located along the edges of the nine overlapping orbits were composited by the mapping program. Radiation data from orbits 3195 to 3202 were not permitted to cross later passes over Central Asia and the Indian Ocean, as this would have caused a 12 hour data time discrepancy in the analysis.

Table 1

Corrections for Instrumental Degradation of TIROS VII, Channel 2 Measurements for Orbits 3195 through 3203.

T_{BB} (°K)	ΔT (°K)
200	+3.8
210	+4.2
220	+4.5
230	+4.8
240	+5.2
250	+5.6
260	+6.1
270	+6.6
280	+7.2
290	+7.6
300	+8.2

The isotherms of channel 2 (8-12 microns) equivalent blackbody temperature, T_{BB} in degrees Kelvin were drawn manually by the analyst for 10 degree temperature intervals. The data were not corrected for instrumental degradation or limb darkening. To obtain more accurate absolute T_{BB} values, the temperature corrections shown in Table 1 should be applied to the uncorrected T_{BB} data (Reference 2). The estimated short-term relative accuracy of the T_{BB} measurements is ±2°K, after application of the degradation corrections shown in Table 1.

The surface weather analyses used during the January and July case studies were based on the best estimate of the synoptic situation from other analyses provided by a number of national weather services. Because of the different orbital inclinations of TIROS VII and TIROS III, the January 21-22, 1964 map (Plate 1) contains data between approximately 70°N and°S, while the July 16, 1961 map (Plate 2) covers the latitudes between 55°N and °S (Reference 3). These are strictly synoptic-radiation analyses of two single and randomly selected days. Thus, it is not possible to derive any climatological or physical conclusions of general seasonal validity from a comparison of these daily maps. However, several radiation features indicate the existence of some major circulation characteristics which are of meteorological interest.

THE TIROS VII AND TIROS III RADIATION ANALYSES OF JANUARY 21-22, 1964 AND JULY 16, 1961

The TIROS VII quasi-global radiation chart for January 21-22, 1964 (Plate 1) shows the equivalent blackbody temperature (T_{BB}, °K) pattern of outgoing "window" radiation (8-12μ) from the earth's surface and the clouds above it during the northern hemisphere winter and southern hemisphere summer. The cold areas which lie poleward of the 35°N and 40°S parallels are related to extratropical cyclonic activity; those near the equator indicate high cloud systems associated with the intertropical convergence zone. This zone is distinguished in the radiation data as an almost continuous belt between Africa and the eastern Pacific Ocean. The presence of tropical cyclone "Danielle" under the high cloud shield at 40°S, 65°E indicates the beginning of hurricane activity in the southern hemisphere.

An interesting synoptic-radiation comparison can be made between the two similarly constructed maps of outgoing radiation shown in Plates 1 and 2. The northern hemisphere is characterized by a large difference in outgoing radiation between winter and summer, while this seasonal difference is comparably smaller over the southern hemisphere. These facts have been documented in the seasonal averages of TIROS VII data where the outgoing radiation changed throughout the year approximately 7 percent at 60°S, but approximately 20 percent at 60°N. At the same latitudes, the outgoing infrared radiation is equal in both winter seasons, but a 13 percent difference exists in the summer seasons (Reference 4). The cloudy zone of the westerlies in the southern hemisphere winter and summer (Plates 1 and 2) begins around 40°S, while a larger latitudinal displacement of the extratropical belt of cloudiness appears during the northern hemisphere winter. An interesting climatological feature is the lack of cloudiness over India and the Southeast Asia region in January as compared to July when the southwest monsoon was very active. The tropical rain belt had shifted far to the south to the Indian Ocean and Indonesia during the northeast monsoon phase of northern hemisphere winter. As was expected the summer time extremes of desert T_{BB} values over the Sahara and Arabian Deserts were not found in Plate 1. Instead of the 300°K values found in these arid areas in July, no value greater than 280°K to 289°K were reported on the January map. In general, the southward displacement of the intertropical convergence zone (ITC) from July to January is readily detectable in Plates 1 and 2. With regard to its high cloud pattern, the ITC appears to be more continuously organized around the world in January than in July. This fact

cannot be generalized by a radiation analysis of only two days. But with the advent of polar orbiting satellites, such as Nimbus and the TIROS Operational System (TOS), the mapping of tropical cloudiness around the world both day and night should make daily and seasonal changes in the structure and intensity of the ITC more easily discernable.

THE RADIATION-SYNOPTIC ANALYSES FOR JANUARY 21-22, 1964

General Discussion

A principal task of this investigation was the synoptic interpretation of the satellite-detected global radiation pattern in terms of a conventional weather analysis. Therefore, world surface synoptic and 500 mb maps were constructed for the period of study. Over areas well covered by conventional meteorological observations, the analysis demonstrates the correlation between the synoptic weather pattern and the satellite information. Over the sparse data areas, the radiation and television data are tested in light of current weather concepts for completeness and continuity.

Global surface weather maps covering the area 75°N and °S were plotted for the 1200 GMT, January 21, 1964, and 0000 GMT January 22, 1964. Figure 2 presents a typical example of world wide surface synoptic data coverage. However, not all of these data are available for a real-time synoptic analysis. The northern hemisphere appears to be fairly well covered by continental and maritime surface observations, but south of 40°S and over the tropical oceans, few synoptic observations are available. Figure 2 documents the necessity for new and unconventional observation techniques such as satellite-borne systems for world synoptic coverage. Figures 3 and 4 are the surface weather analyses of the conventional surface observations plotted at 1200 GMT, January 21, and 0000 GMT, January 22, 1964. The TIROS VII radiation data were used to infer the weather analysis over the remote Southern Hemisphere oceanic regions where data were sparse. All available TIROS VII and VIII television coverage was used for confirmation and completeness of the surface analysis.

Detailed Analysis

The January 21-22, 1964 period represents the typical mid-seasonal circulation of northern hemisphere winter and southern hemisphere summer. Strong cyclones are located over the North Atlantic and North Pacific Oceans, while anticyclones mainly influence the weather over western and southern Europe, central Canada, east-central Asia, and the United States (Figures 3 and 4). Northern Europe is affected by maritime air masses, protruding far into Russia with extensive cloudiness and precipitation. The number of secondary warm fronts on the surface map is not reflected in the radiation pattern, but the main warm front extending from northern Germany eastward into the continent is substantiated by the infrared data. Figure 5 is a TIROS VII television mosaic and nephanalysis which shows the heavy cloudiness surrounding a developing vortex at 57.5°N and 50°E at 0600 GMT on January 22, 1964. This singular vortex is not distinctively seen in the radiation data or in the synoptic analysis. It appears to be part of a complex system of vortices and fronts over central Russia.

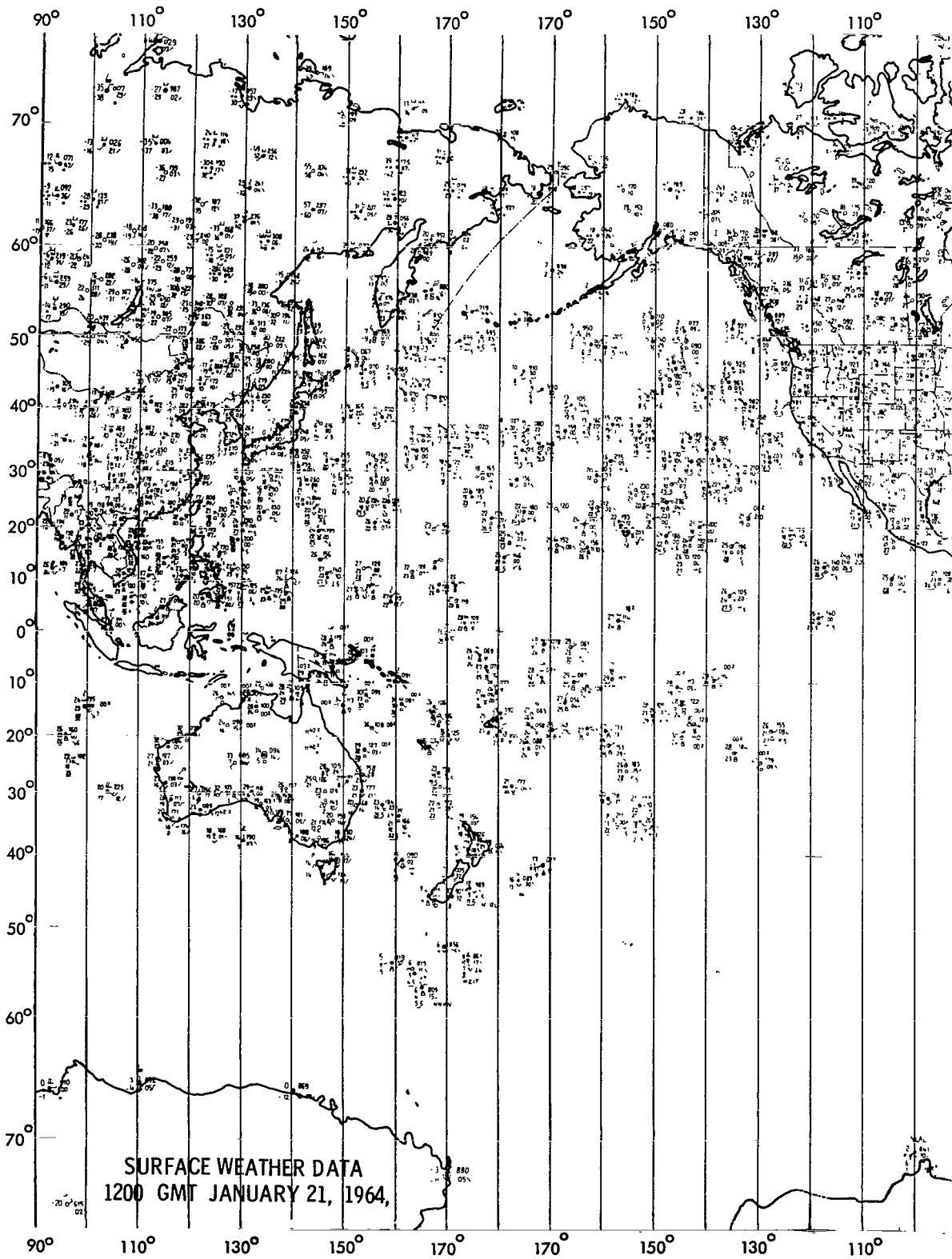
90°
110°
130°
150°
170°
170°
150°
130°
110°
70°
60°
50°
40°
30°
20°
10°
0°
10°
20°
30°
40°
50°
60°
70°
SURFACE WEATHER DATA
1200 GMT JANUARY 21, 1964,

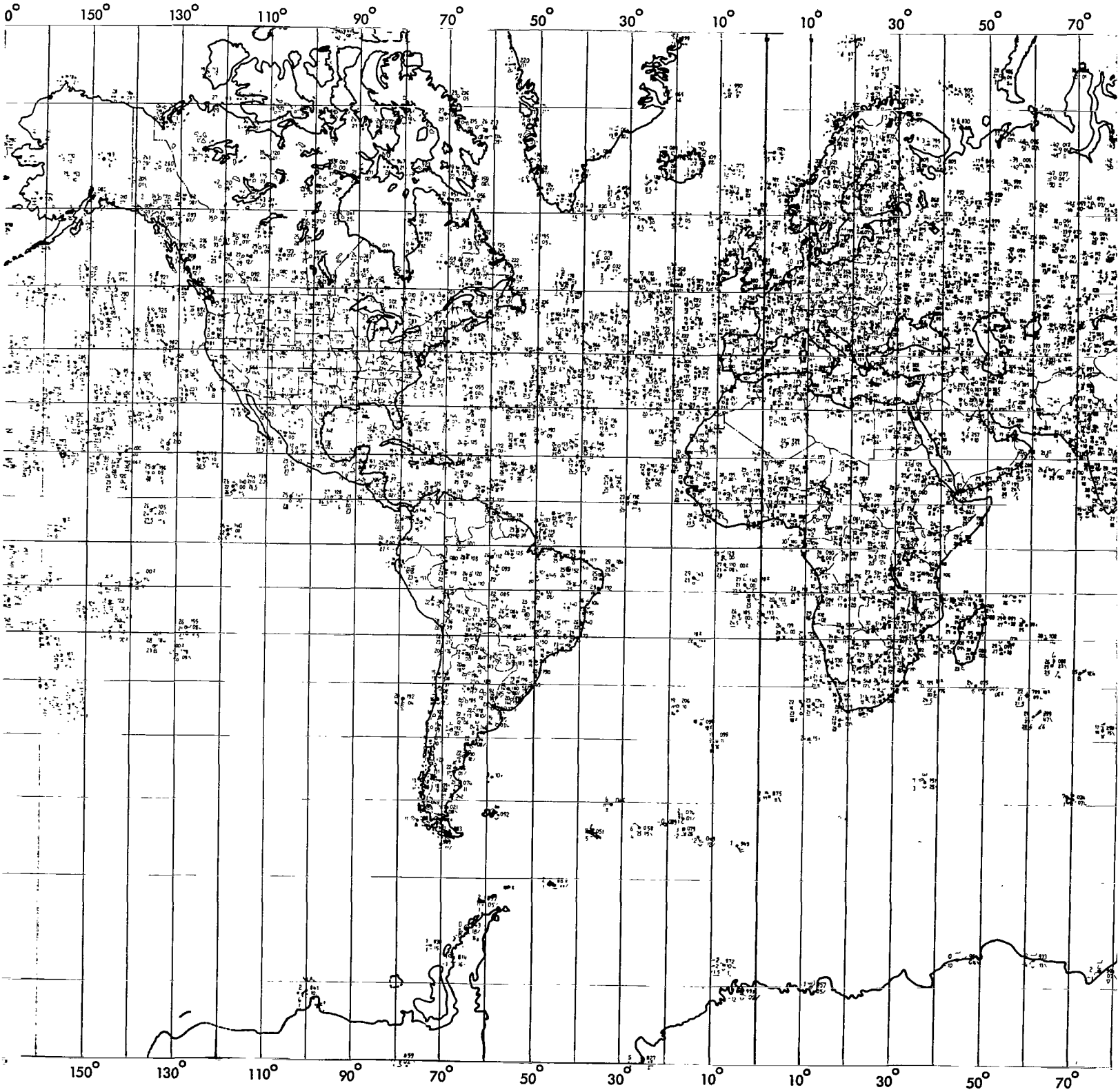

Figure 2–Surface weather data, 1200 GMT,

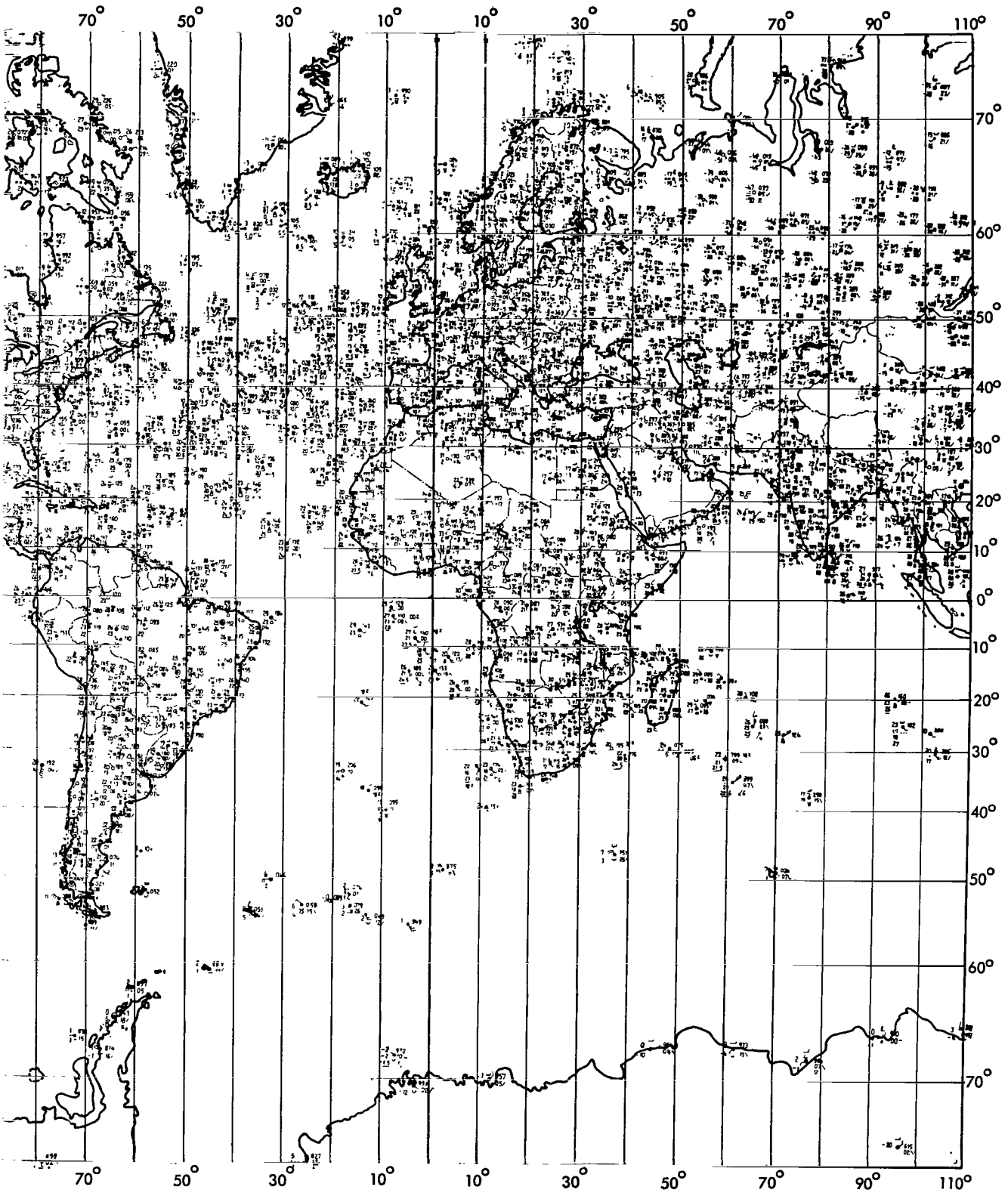

Figure 2–Surface weather data, 1200 GMT, January 21, 1964.

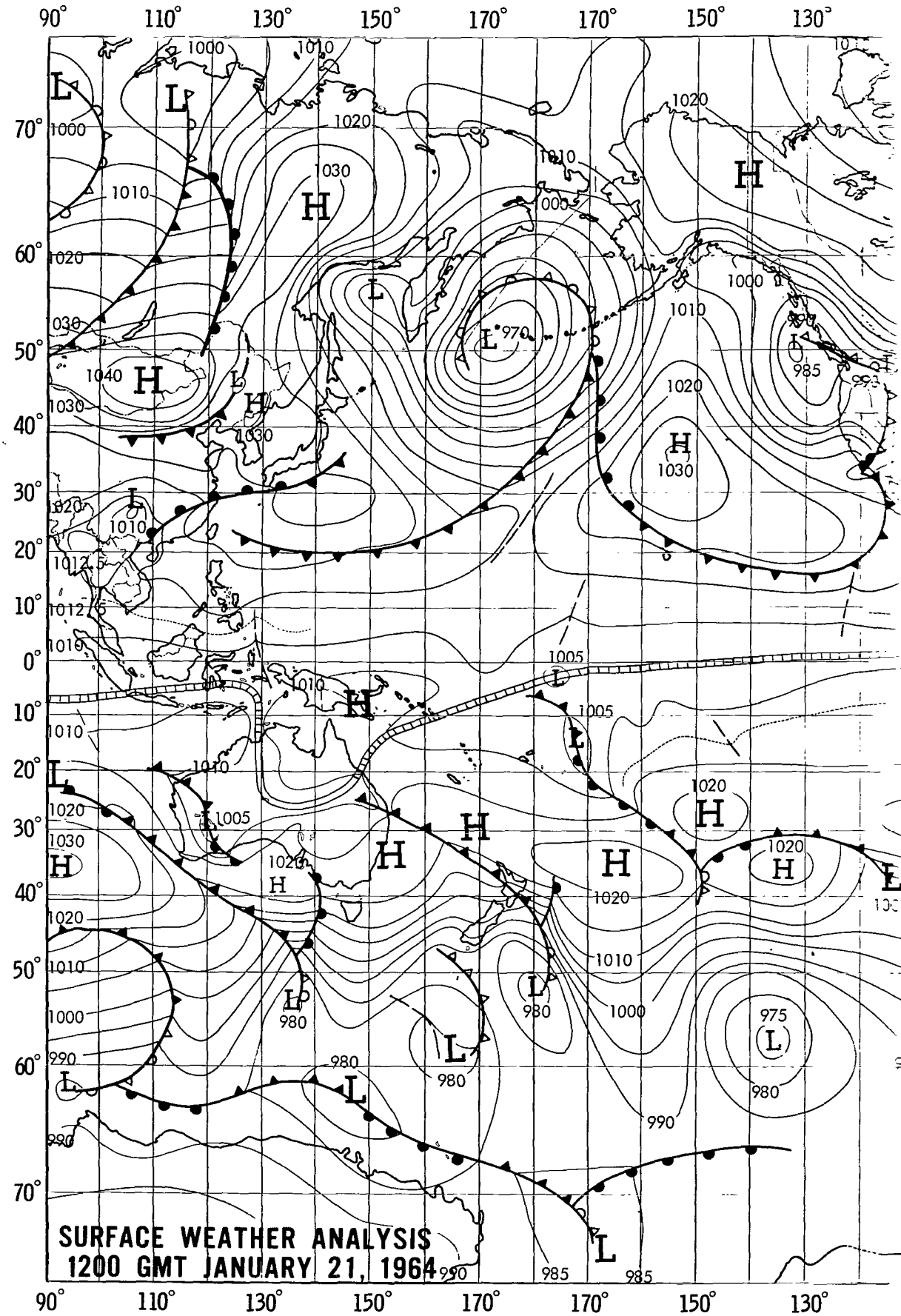
90° 110° 130° 150° 170° 170° 150° 130°
70° 60° 50° 40° 30° 20° 10° 0° 10° 20° 30° 40° 50° 60° 70°
SURFACE WEATHER ANALYSIS
1200 GMT JANUARY 21, 1964

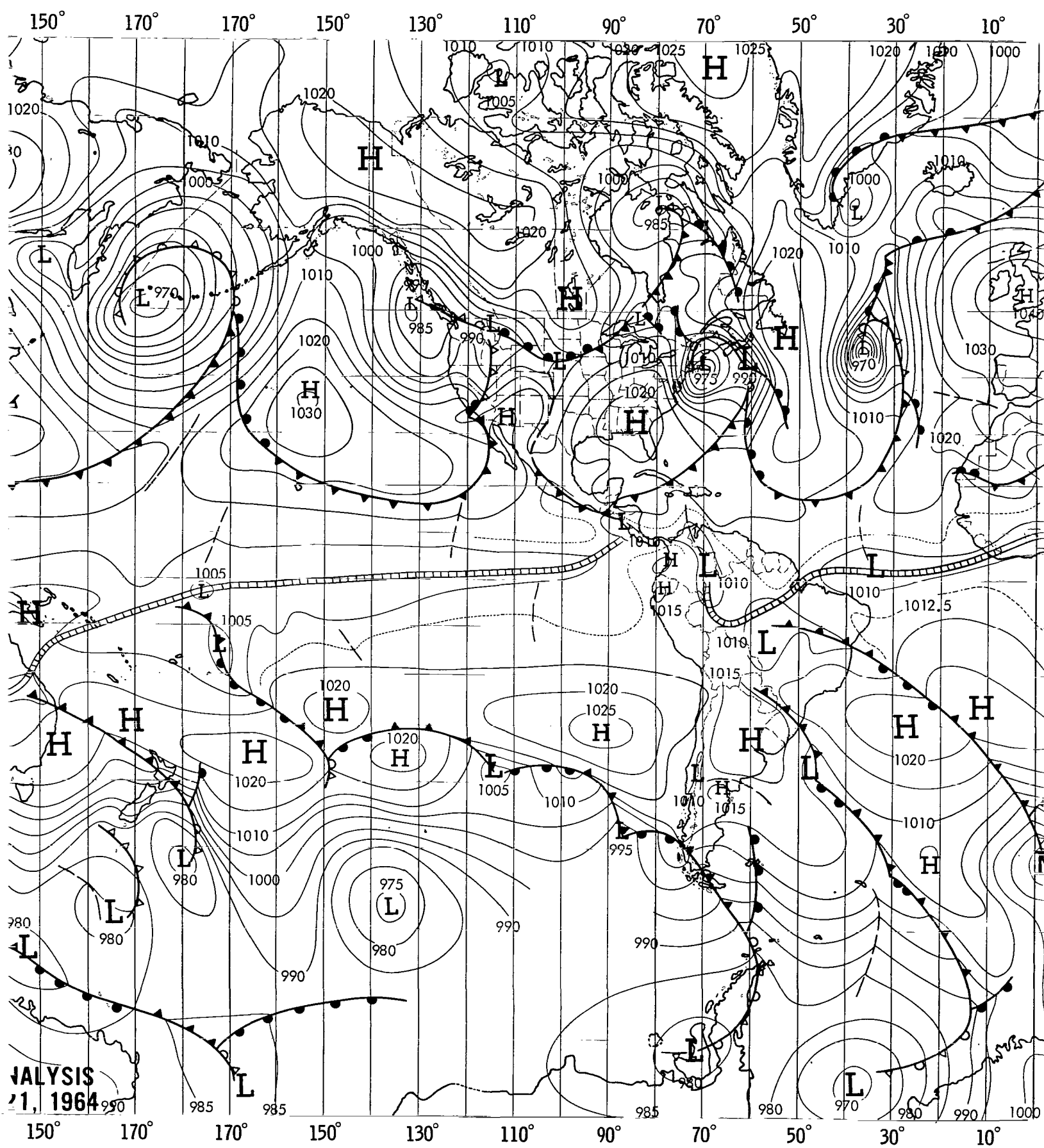
150° 170° 170° 150° 130° 110° 90° 70° 50° 30° 10°
NALYSIS
21, 1964

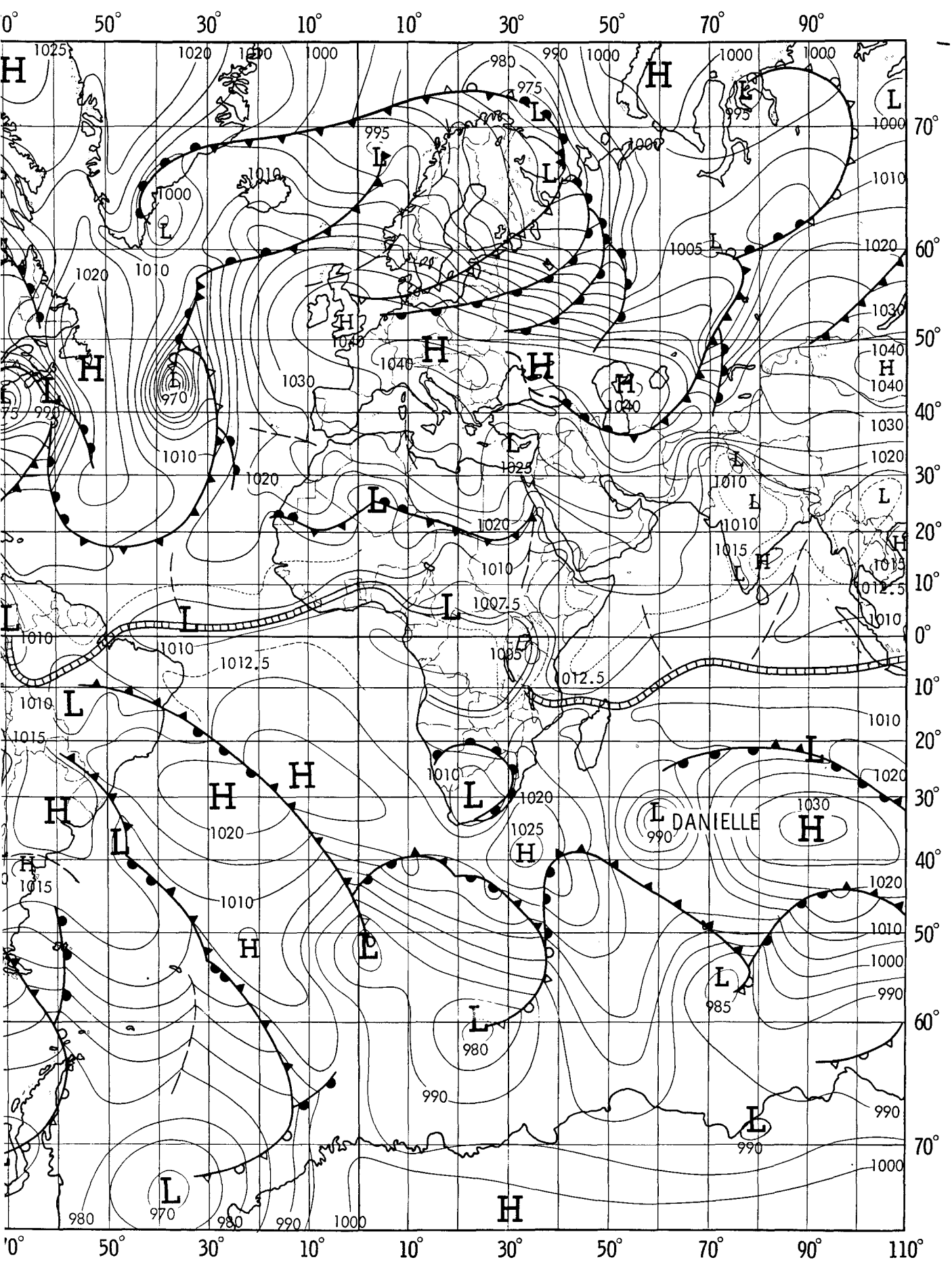

Figure 3—Surface weather analysis, 1200 GMT, January 21, 1964.

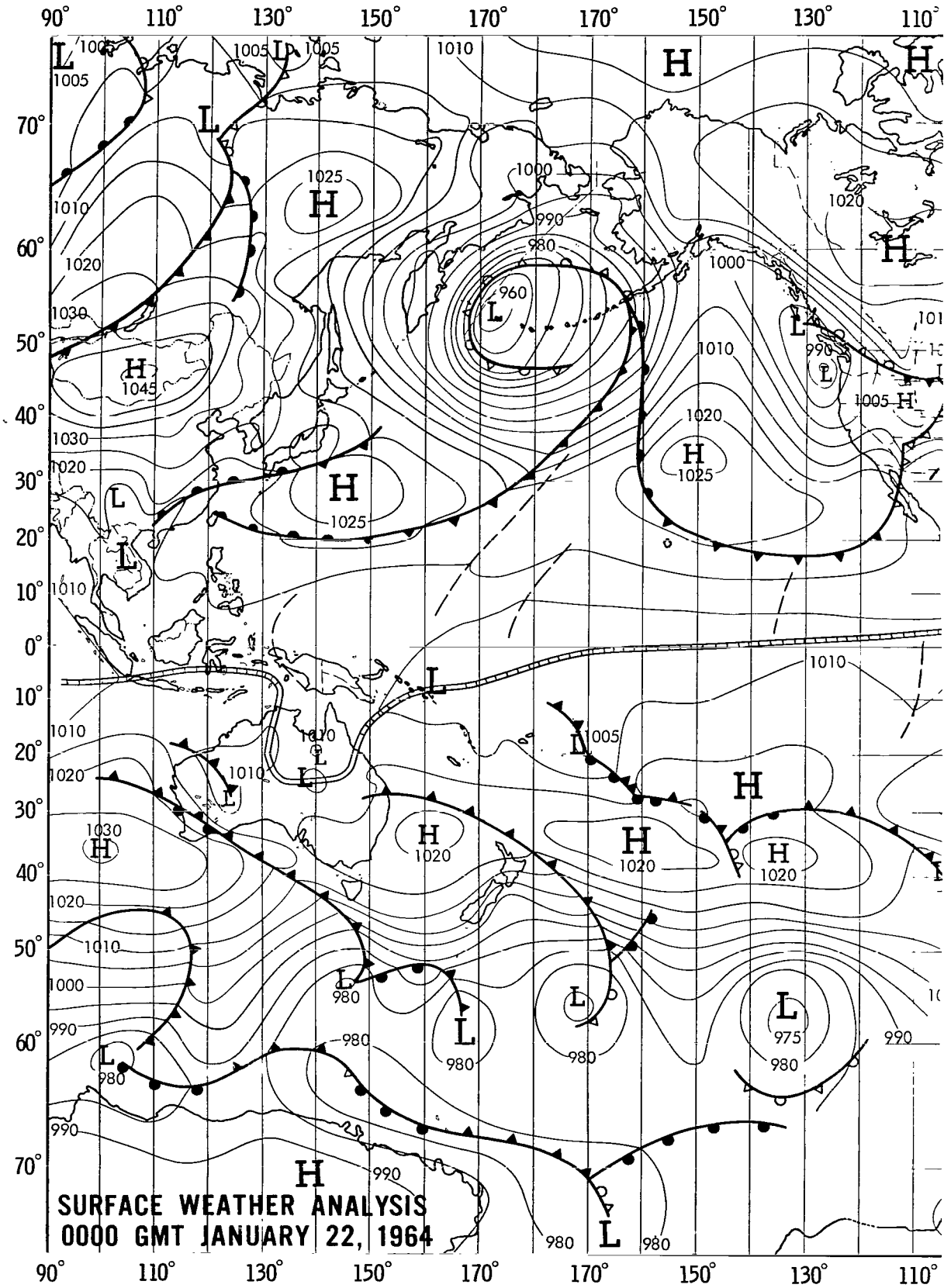
90° 110° 130° 150° 170° 170° 150° 130° 110°
70° 60° 50° 40° 30° 20° 10° 0° 10° 20° 30° 40° 50° 60° 70°
SURFACE WEATHER ANALYSIS
0000 GMT JANUARY 22, 1964

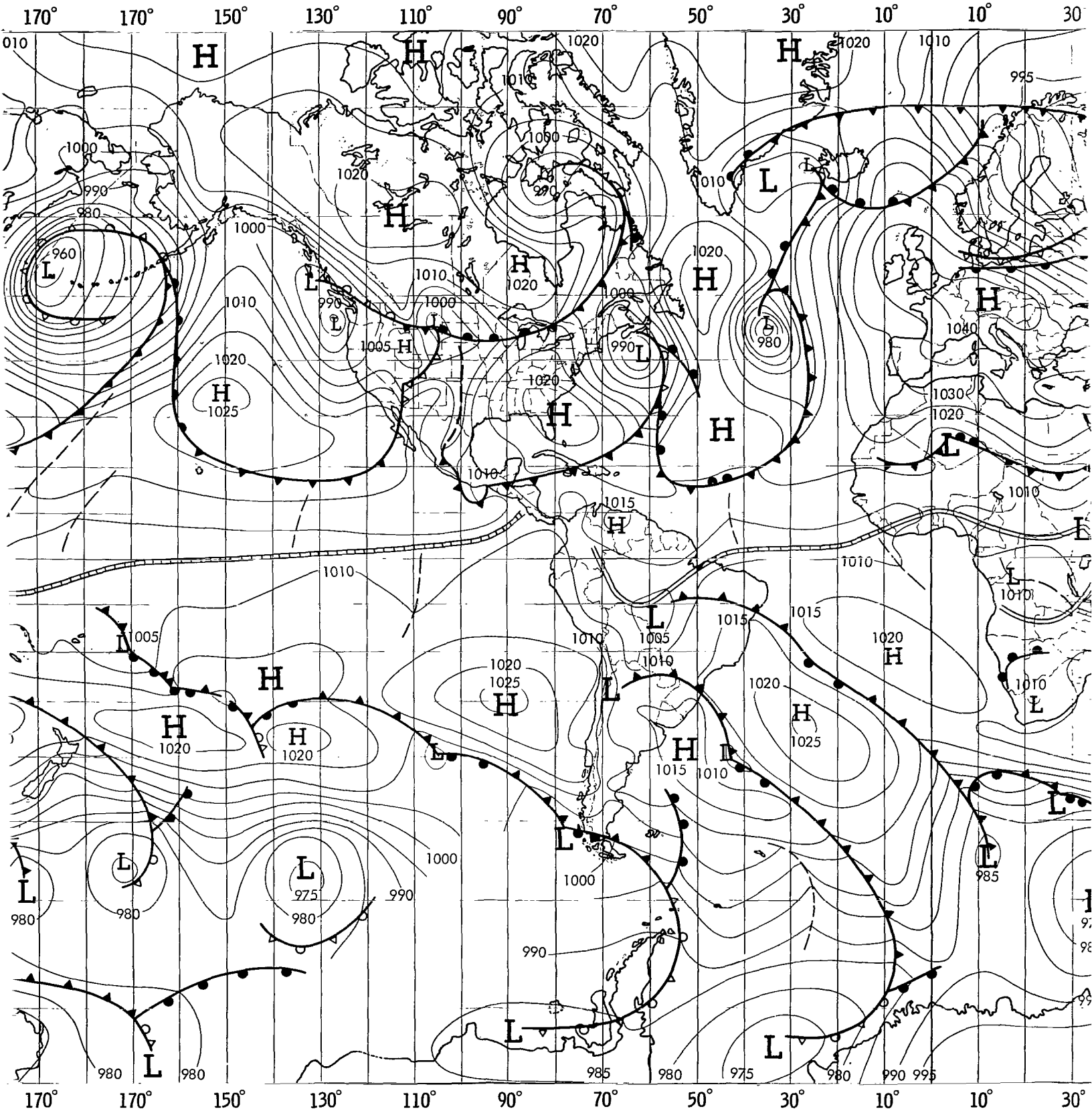

Figure 4—Surface

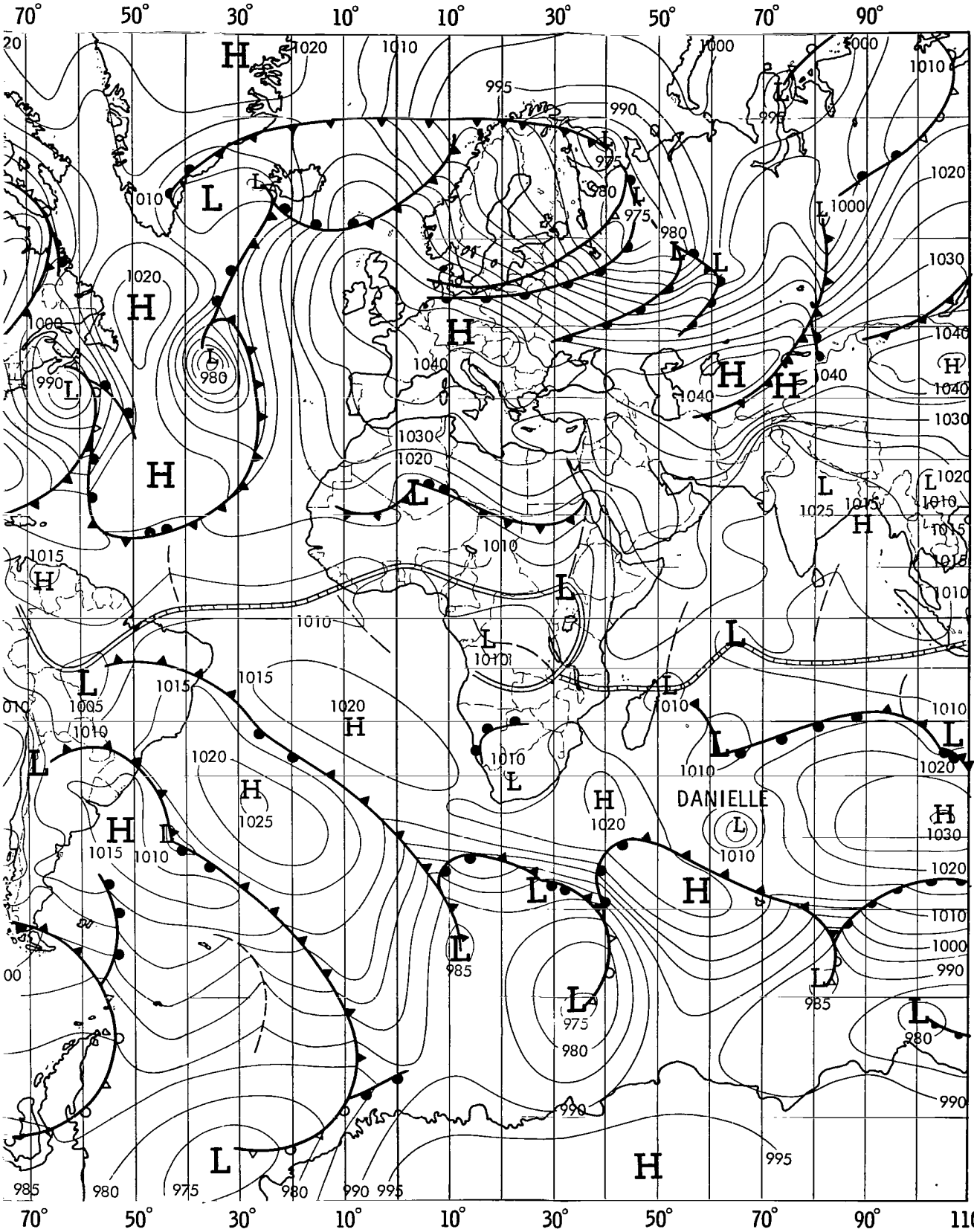

Figure 4—Surface weather analysis, 0000 GMT, January 22, 1964.

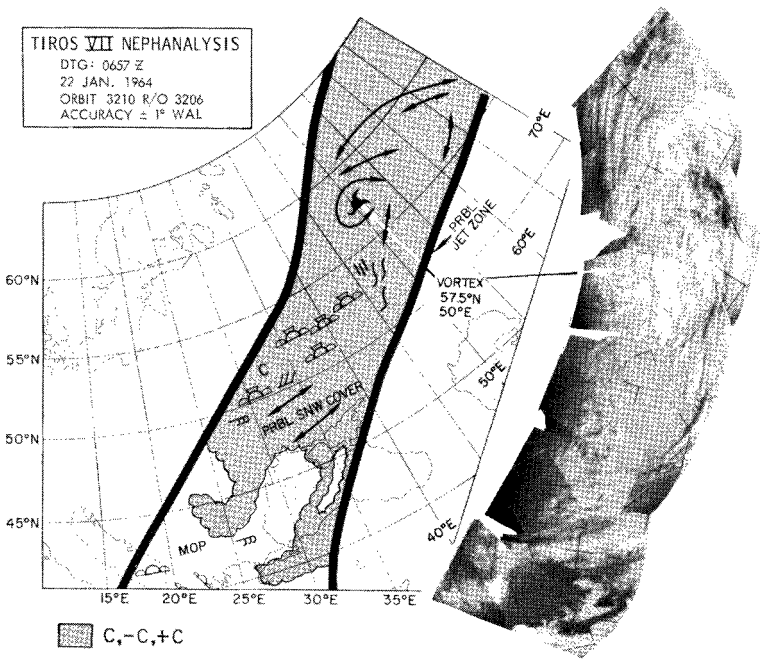

Figure 5—Mosaic of TIROS VII television pictures and nephanalysis over Russia on January 22, 1964.

Over the Atlantic Ocean, there are some radiation data gaps within the areas of the two major cyclones (off the U. S. east coast and northwest of the Azores). The open wave cloud system north of the mid-Atlantic cyclone which extends toward Iceland is well indicated by the radiation data. The cold front west of Norway is only weakly represented in Plate 1, but the surface trough over Norway, shown in Figure 3 with its numerous cumulonimbus clouds and showers, is well reflected by a band of T_{BB} values below 240°K.

Over the North Pacific, one large extratropical cyclone dominates the synoptic pattern. The spiraling occlusion and the cold and warm frontal regions are supported by the radiation analyses (Figure 6). Figure 7 shows TIROS VII television mosaic and nephanalysis over the occlusion at 2200Z on the previous day. The western portion of the cold front cannot be easily detected west of 25°N, 170°E in Figure 6 because of the weak appearance of the front in an anticyclonic surface flow. A new area of cyclogenesis is seen forming as an open wave, southwest of Japan. This is indicated in Figure 6 by the high cold clouds with T_{BB} values below 240°K. The large comma-shaped area of "Kona" storm high clouds south of Hawaii, as indicated in Figure 6, is located under the anticyclonic ridge ahead of a 300 mb trough west of Hawaii. The cold high clouds relating to the ITC can be seen over Borneo and New Guinea extending from 10°N to 10°S across the equatorial west-central Pacific Ocean.

The continents of the northern hemisphere present a problem in the derivation of cloudiness from the "window" radiation measurements because cold surface temperatures under clear sky conditions resemble high cloud radiation. This is the case in the large area of T_{BB} values below

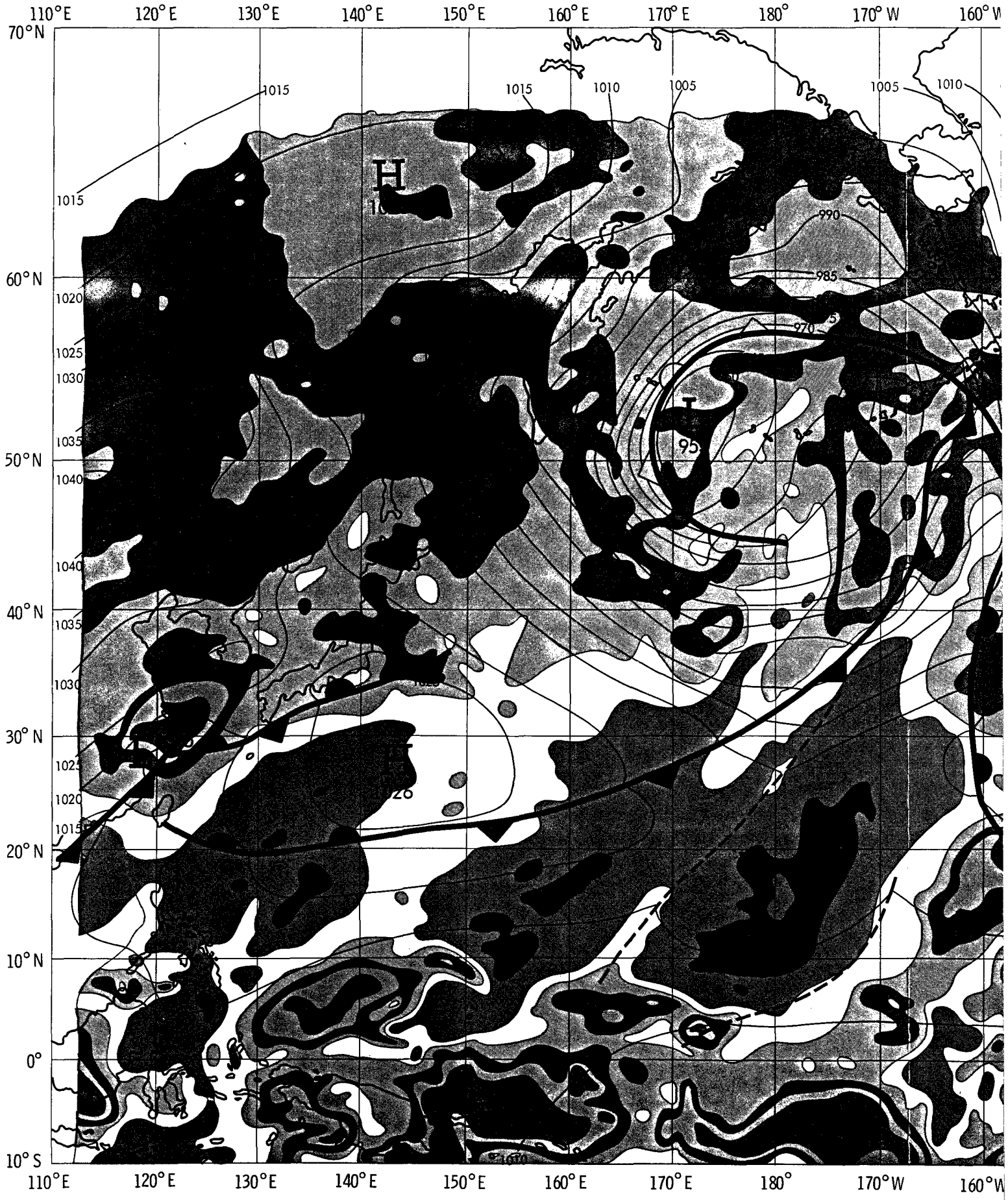

Figure 6 - Composite map of "window" radiation from TIROS VII (Channel 2) for orbits 3197-3203, on Janua
The surface synoptic map that is superimposed was based mainly on the U. S. Weather Bureau, N

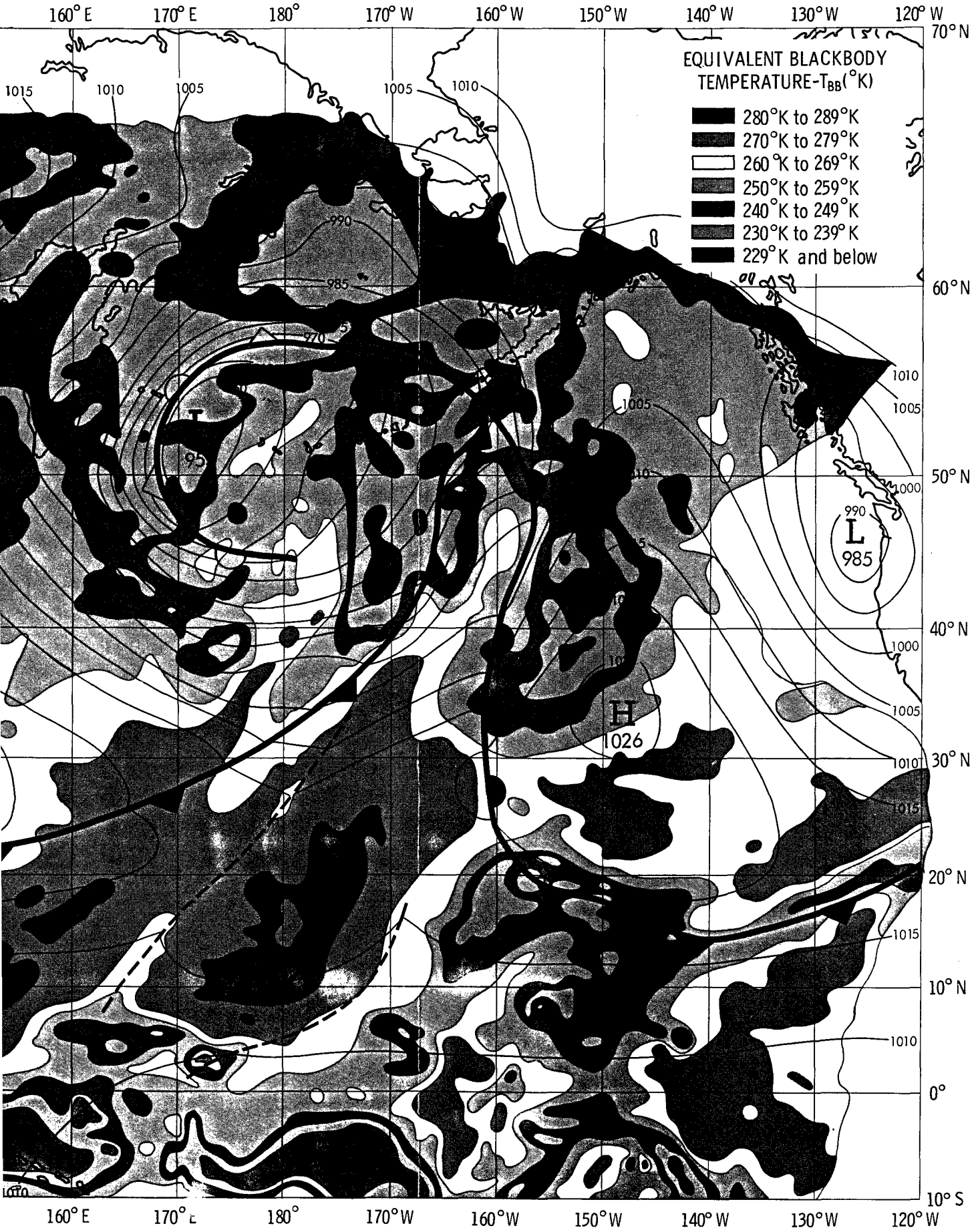

TIROS VII (Channel 2) for orbits 3197-3203, on January 21-22, 1964 over the North Pacific Ocean.
sed was based mainly on the U. S. Weather Bureau, National Meteorological Center analyses.

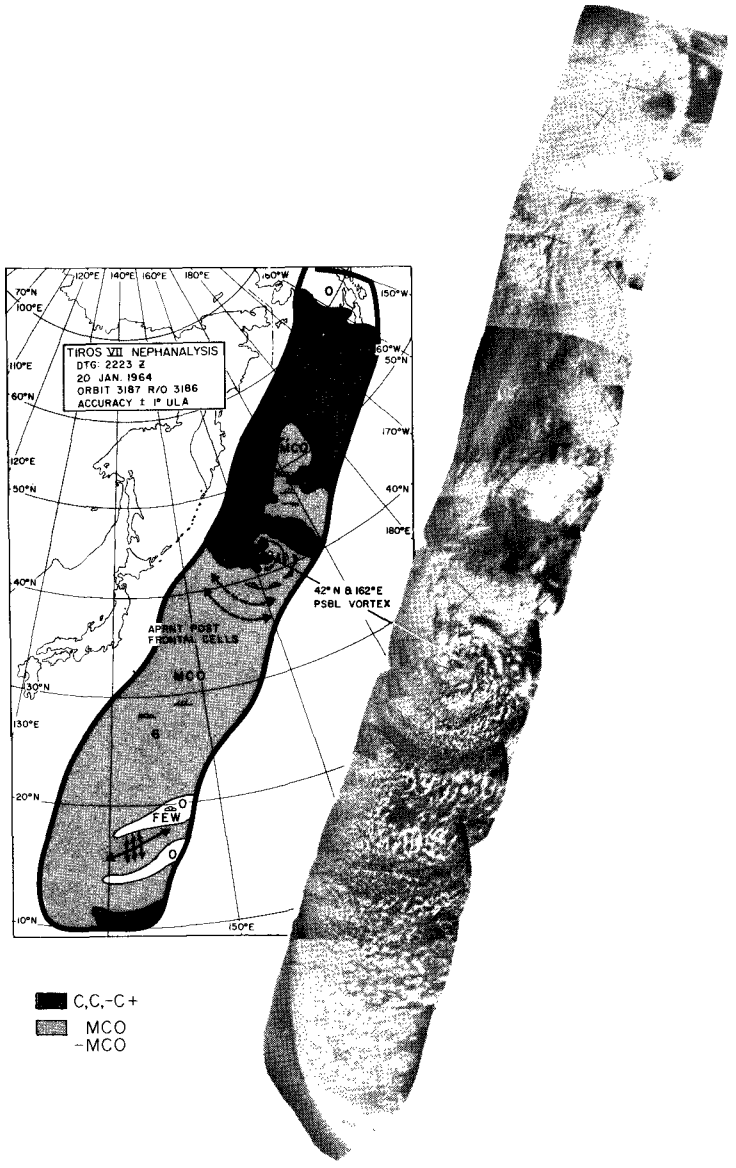

Figure 7—Mosaic of TIROS VII television pictures and nephanalysis over the western Pacific Ocean on January 20, 1964.

240°K (approximately -30°C) over Canada north of 55°N and west of Hudson Bay as well as over northeast Siberia north of 60°N between 130° to 170°E (Plate 1 and Figure 6). Both areas are covered by surface anticyclones and recorded free air temperatures of 230°K for northwest Canada and 220°K in Siberia. Surface observations along the Greenland coasts indicate some cloudiness but within the surface anticyclone over the inland ice, the low T_{BB} values follow the geographical outline of the ice covered island. The same situation may frequently occur over the Antarctic, but on January 21-22, 1964, the low T_{BB} values around 50°E and from 80°E to 110°E, 65°S to 70°S are caused by clouds as suggested by the altostratus or cirrus observed by the weather stations along the coast.

To determine whether any significant climatological features can be derived from TIROS data, a mean January 1964 grid print map of channel 2 (8-12μ) radiation data was printed out by the 7094 computer (Figure 8). A mean cloud cover chart derived from the TIROS VII television nephanalyses for the same period was also constructed (Figure 9). A comparison of these two charts, shows heavy cloudiness relating to the ITC position in the eastern Pacific Ocean, from approximately 5°N to 25°N. The broken to overcast clouds in Figure 9 are indicated by the 260K to 275K T_{BB} values. The subtropical high pressure system with its scattered cloud areas from 5°N to 15°S is also indicated by the 280K to 285K isotherms. There is some evidence of mismatching of cloud amounts and T_{BB} values in the 150°W to 160°W region. Since the monthly channel 2 data include day and night cloud regimes, diurnal cloud effects and the presence of 5/10 middle and high cloudiness may help explain this discrepancy. The results of this brief climatological comparison show that large scale cloud features can be delineated by monthly TIROS data in a manner similar to conventional weather data.

The 500 mb chart (Figure 10) reflects the general northern hemisphere surface pressure pattern with a strong blocking anticyclone over Europe with polar vortices over northern Canada, northern Siberia, the north Pacific, and the north Atlantic. The polar jet stream band circles the globe over mid-latitudes, while a more southerly subtropical jet passes over the northeast coast

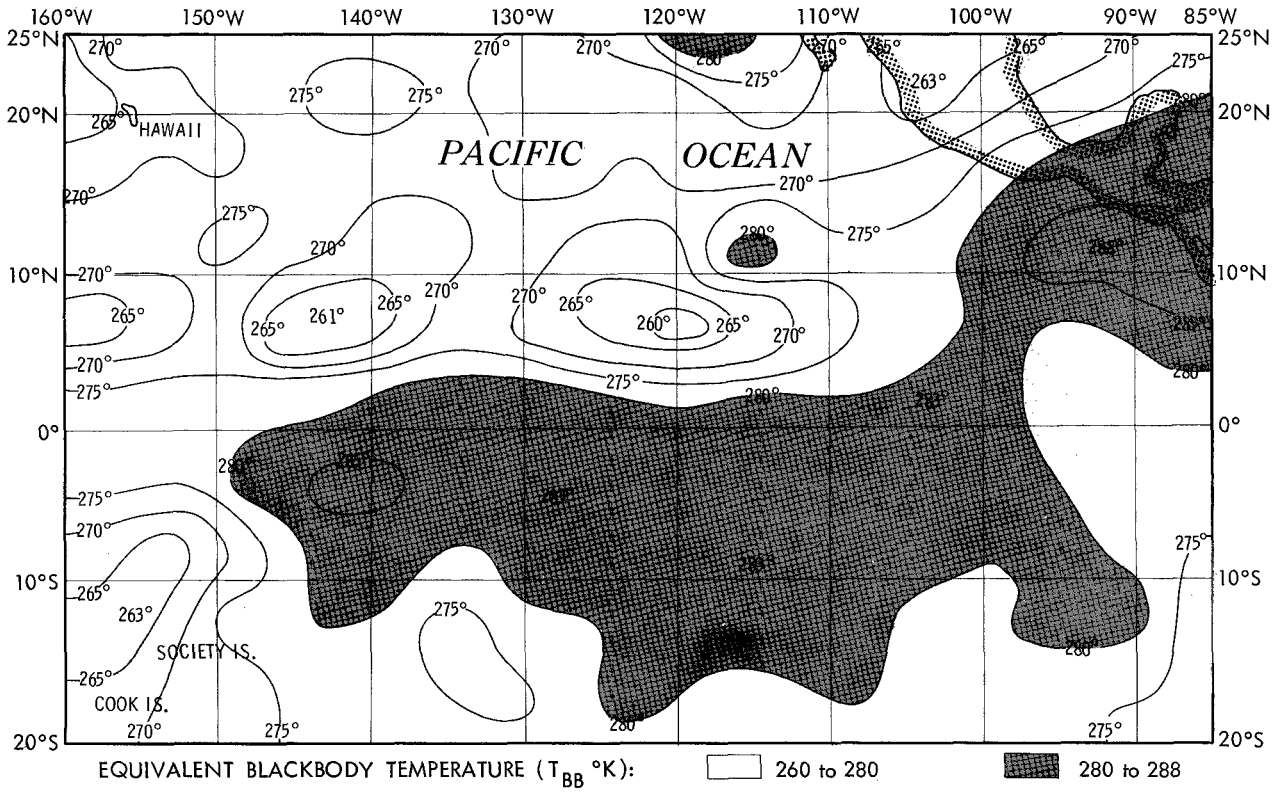

Figure 8—Mean monthly composite map of "window" radiation (Channel 2, 8-12μ) from TIROS VII for January 1964 over the eastern Pacific Ocean.

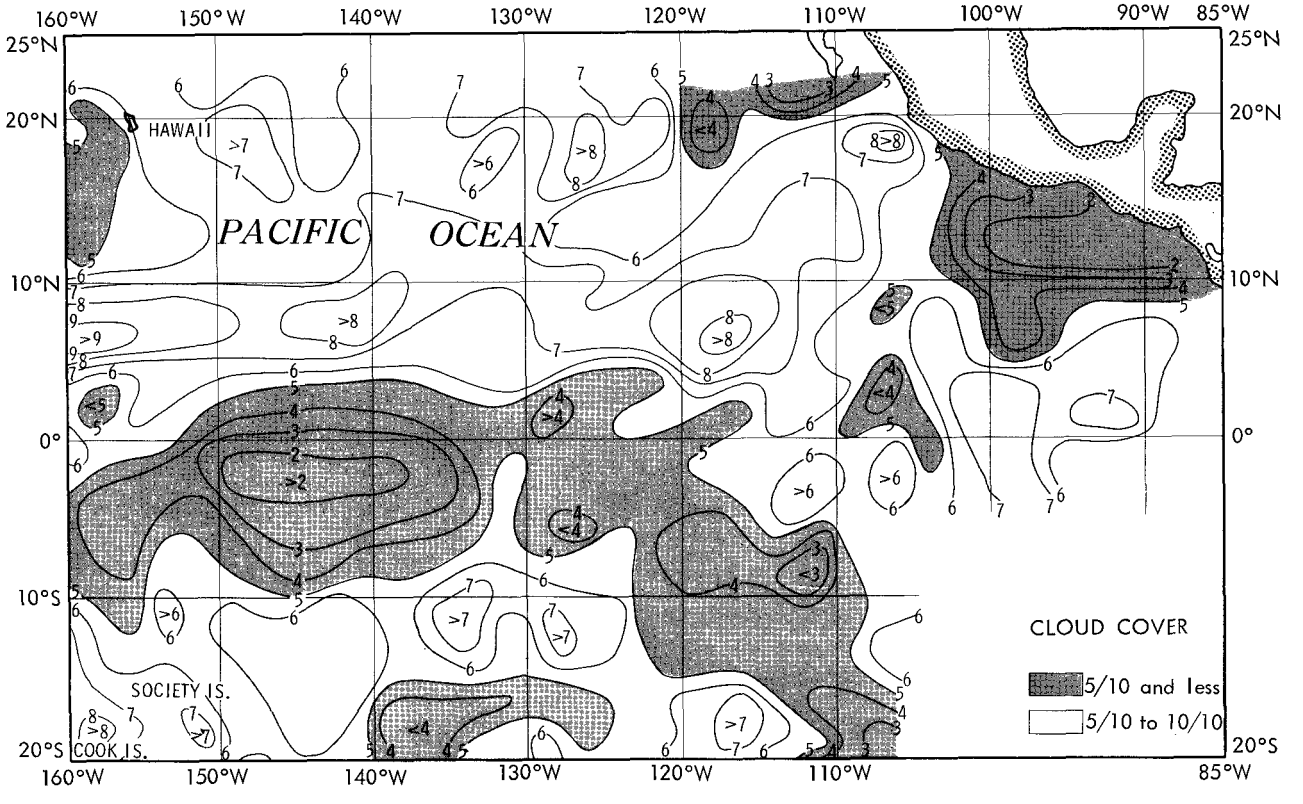

Figure 9—Mean monthly cloud cover chart derived from TIROS VII television nephanalysis for January 1964 over the eastern Pacific Ocean.

of Africa, north-central India, and southern China. The intertropical convergence zone can be traced at the same approximate location as shown on the surface weather maps. The southern hemisphere jet stream is shown traveling in varying directions along the 40°S to 60°S latitude circles in good synoptic correspondence to the location of surface frontal systems.

An interesting feature of the southern hemisphere summer circulation is suggested by the January 21-22, 1964 radiation map (Plate 1). Long and nearly continuous bands of high reaching clouds (T_{BB} values < 240°K) extend from high southerly latitudes deep into the subtropics where they appear to merge with the intertropical front. This can be seen over the South Atlantic Ocean to east-central Brazil, in the northeastern Australian region, and east and north of the Samoan Islands. The subtropical high pressure belt is generally located between 20°S and 40°S while the mid-latitude storm track is represented by a large number of cyclones between 40°S and 60°S (Plate 1, Figures 3 and 4).

A frontal system is shown passing the southernmost part of Chile and Argentina with intense cloudiness, indicated by T_{BB} values below 250°K (Plate 1). The trough line passing the island of South Georgia at 54°S, 38°W is also indicated by low T_{BB} values. This trough is separated from the preceding cold front which extends from the Weddell Sea northwestward into southern Brazil.

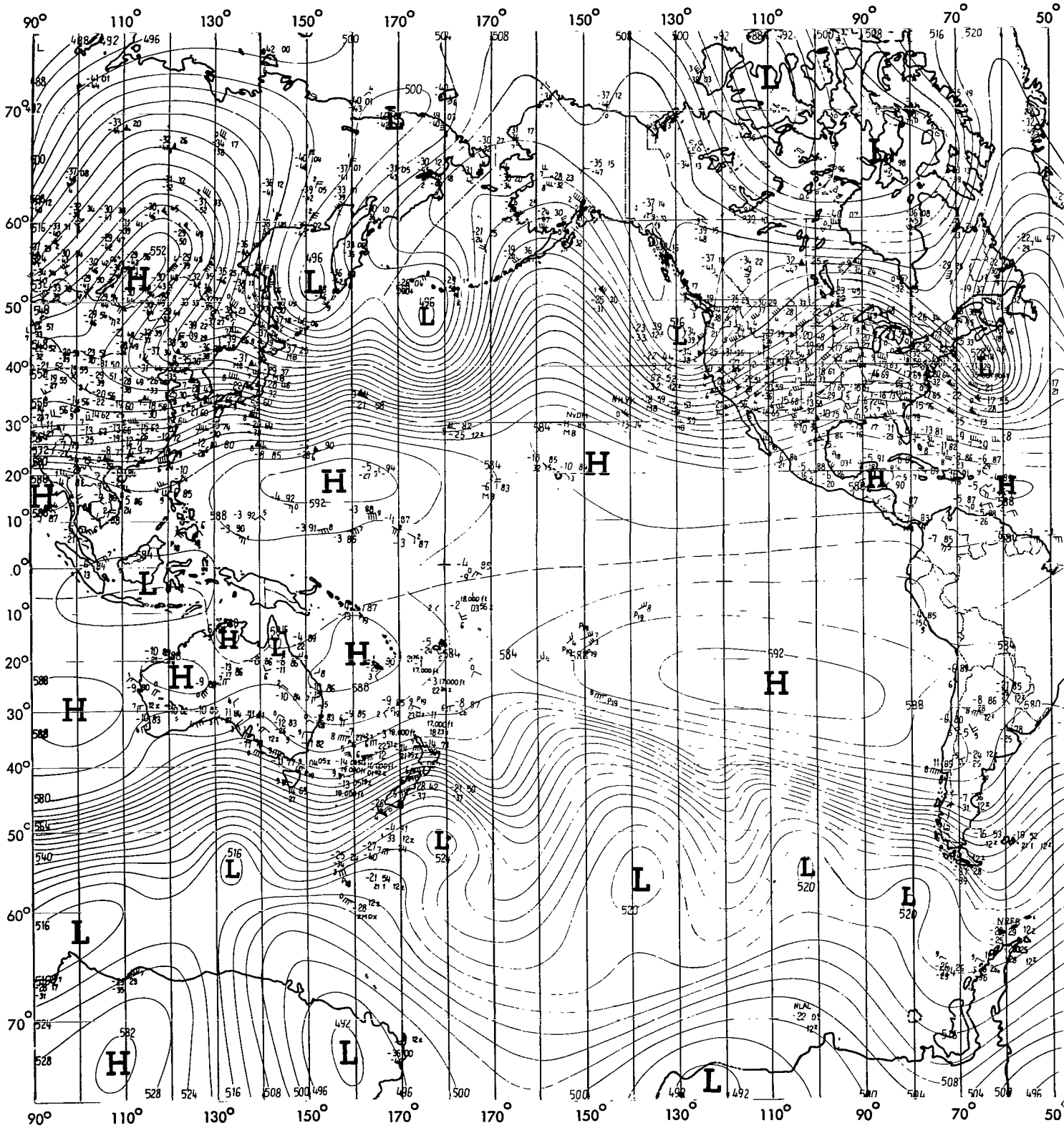
90° 110° 130° 150° 170° 170° 150° 130° 110° 90° 70° 50°
70° 60° 50° 40° 30° 20° 10° 0° 10° 20° 30° 40° 50° 60° 70°

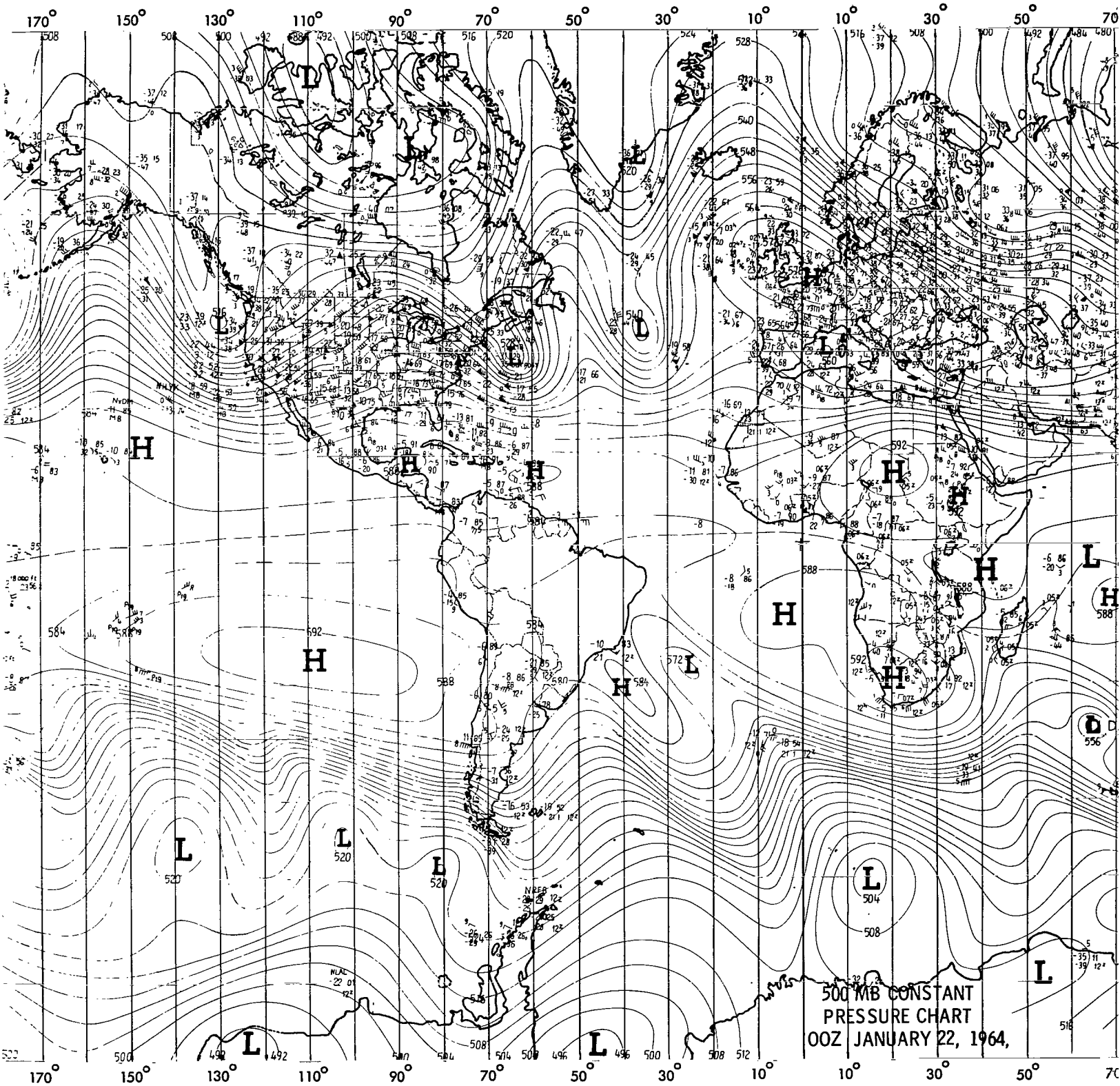

Figure 10–500 mb constant pressure chart; 0000

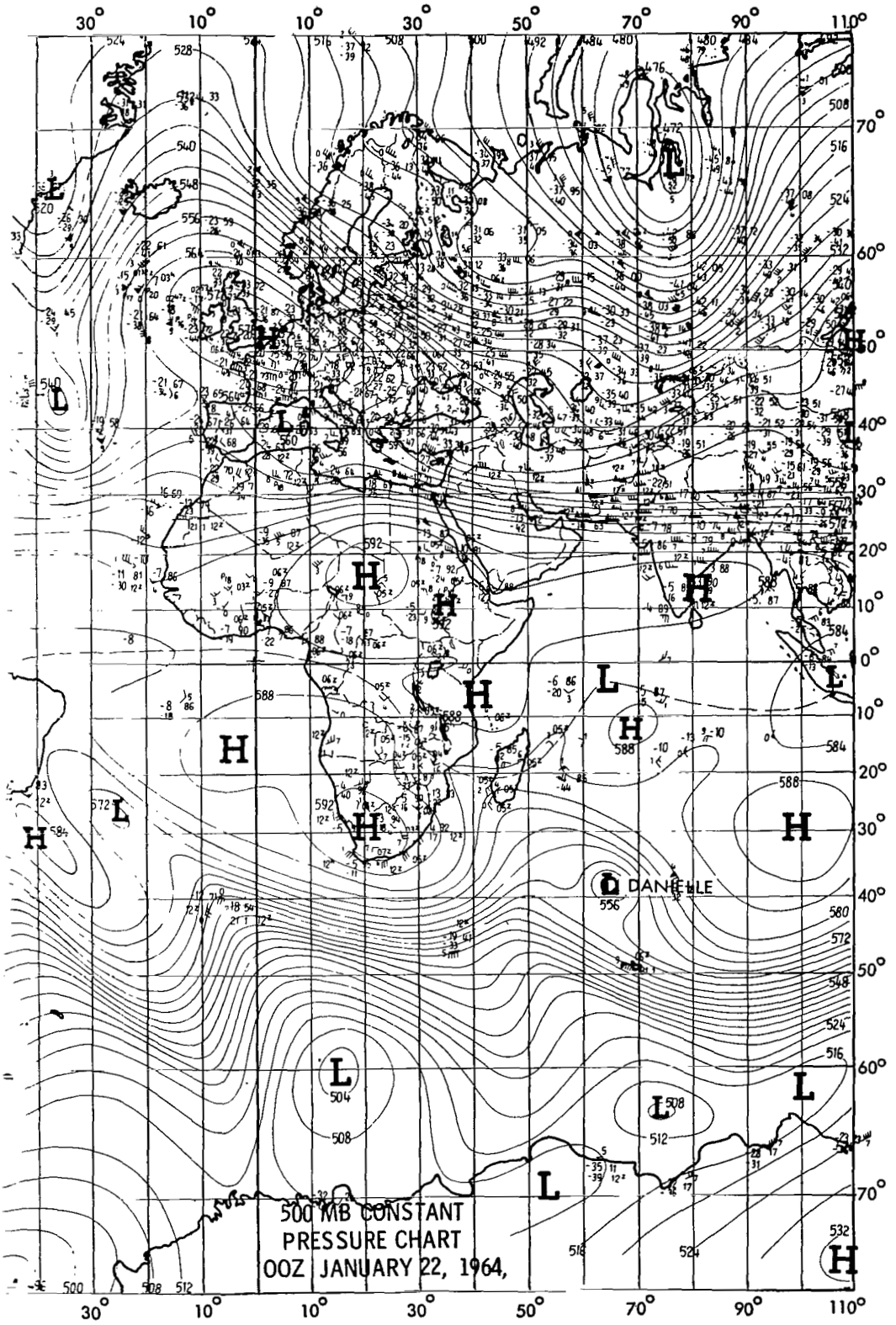

Figure 10–500 mb constant pressure chart; 0000 GMT, January 22, 1964.

Figure 11 is a TIROS VIII television mosaic and nephanalysis which shows a portion of this frontal system on 20 January 1964. The synoptic patterns over Brazil indicate that the South American ITC lies south of the Amazon River where it is shown on the radiation map (Plate 1). A long frontal system extends northwestward from the tip of South America across the Pacific Ocean until it merges with the ITC at 180° longitude. This synoptic interpretation (shown in Figures 3 and 4) was inferred from the radiation pattern in Plate 1 and supported by television pictures and nephanalysis (Figure 12). In the low latitude region of Figure 12a, portions of the South Pacific front can be seen in orbits 444-446, from 35°S, 110°W, to 32°S, 140°W, to 30°S, 170°W, and then turning northward toward 8°S, 180° longitude. Extensive frontal clouds are closely connected with the large cloud mass of tropical cyclone "Danielle" at 30° to 35°S, 62°E (Figures 12 and 13). This cyclone had moved to the southeast from the vicinity of the Malagasy Republic and is seen merging with a mid-latitude storm. The cyclonic system south of Cape Town, South Africa appears intensively in the radiation data (Figure 13), in television pictures (Figure 11), and in the surface and upper air observations (Figures 3, 4, and 10). TIROS VIII television mosaics and nephanalyses on January 21 and 22, 1964 shown in Figure 14, contain more details about the cloud systems which extend in a circumpolar direction from the Indian Ocean to the South Pacific Ocean.

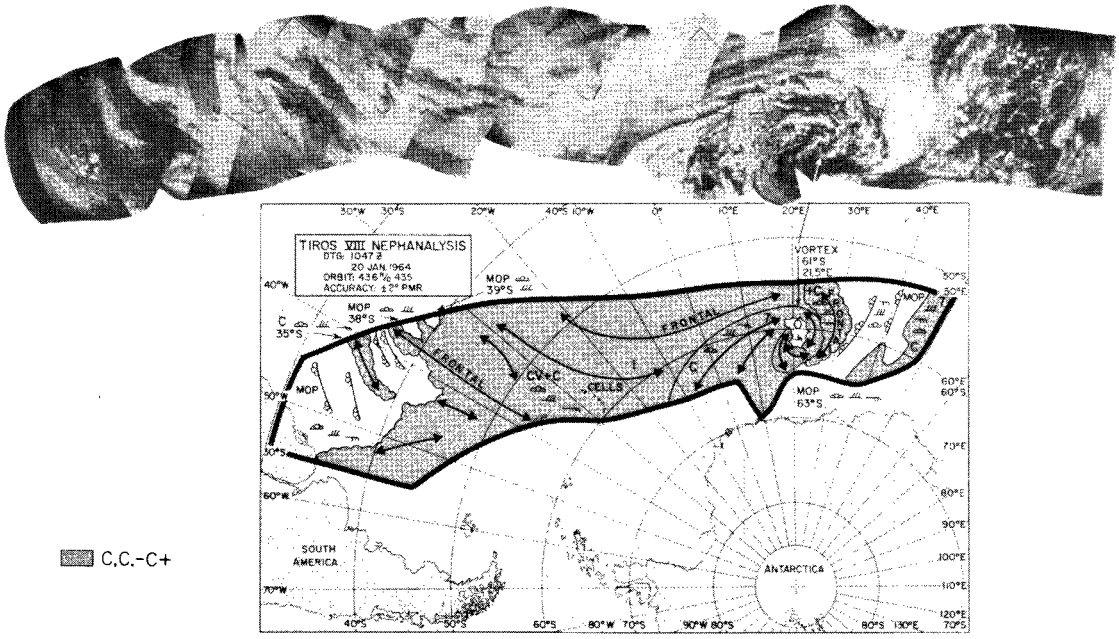

Figure 11—Mosaic of TIROS VIII television pictures and nephanalysis on January 20, 1964, southeast of South America.

The synoptic conditions over tropical Africa appear to be quite complicated. The humid equatorial air over the Congo Basin shows distinct boundaries along the dry air masses from the Sahara Desert to the north, the dry air over South Africa, and the maritime air from the Indian Ocean (Figures 3 and 4) (Reference 5). The heavy cloudiness (cold T_{BB} values < 240°K) shown in Figure 13 is centered between these areas approximately along the weak surface trough, wind convergence zone, and the 500 mb trough (Figure 10).

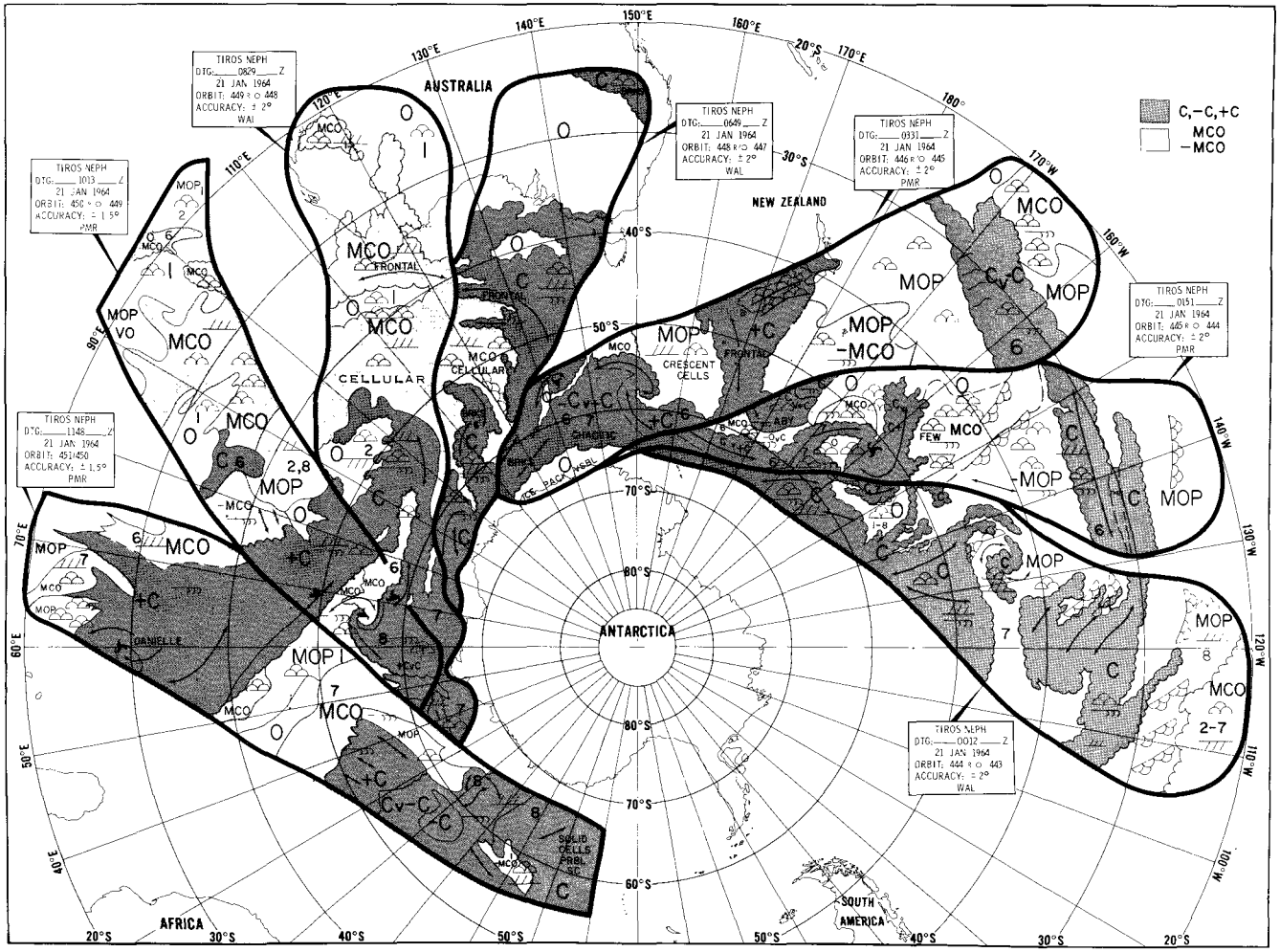

Figure 12a—Nephanalysis of TIROS VIII television pictures on January 21, 1964, in the Southern Hemisphere.

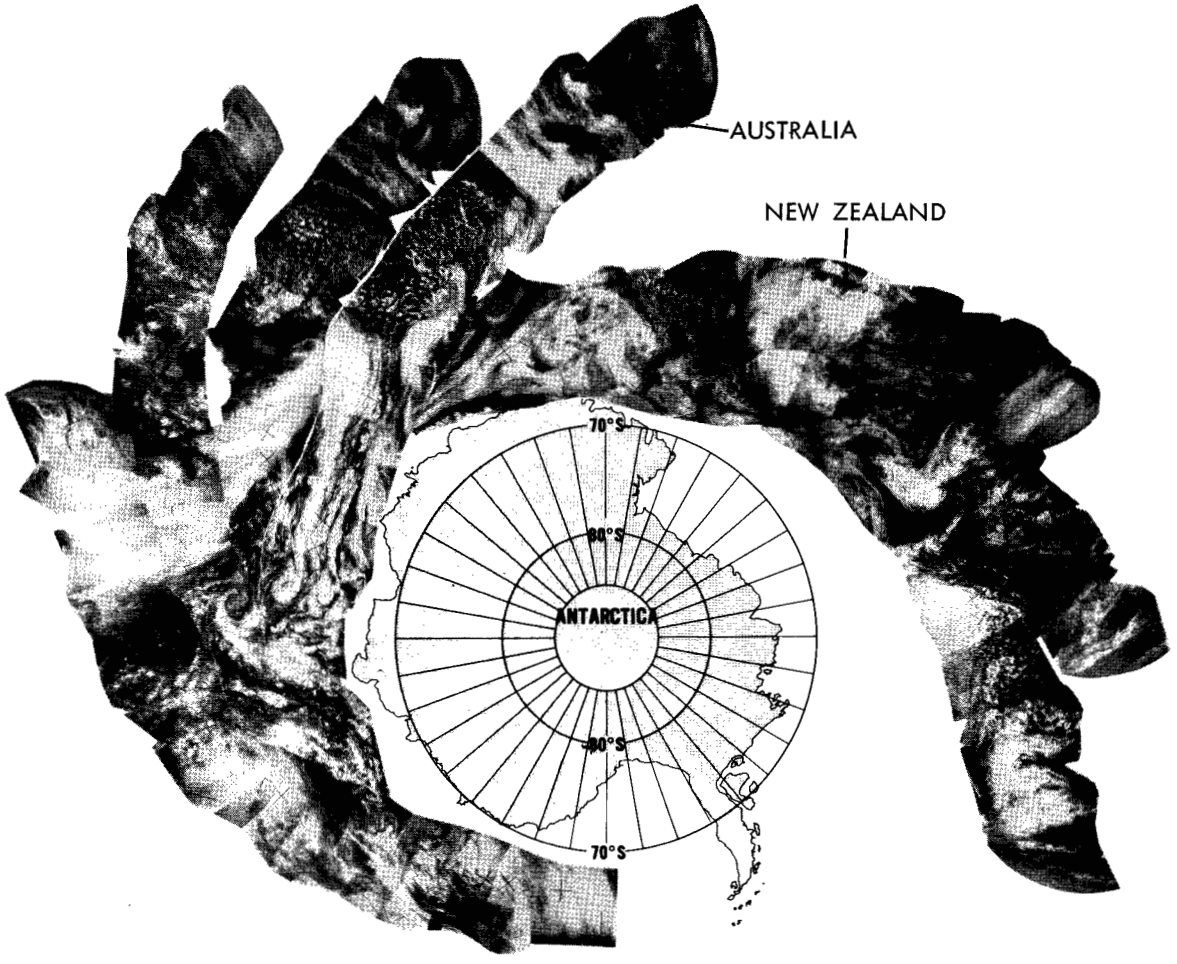

Figure 12b—Mosaic of TIROS VIII television pictures on January 21, 1964, in the Southern Hemisphere.

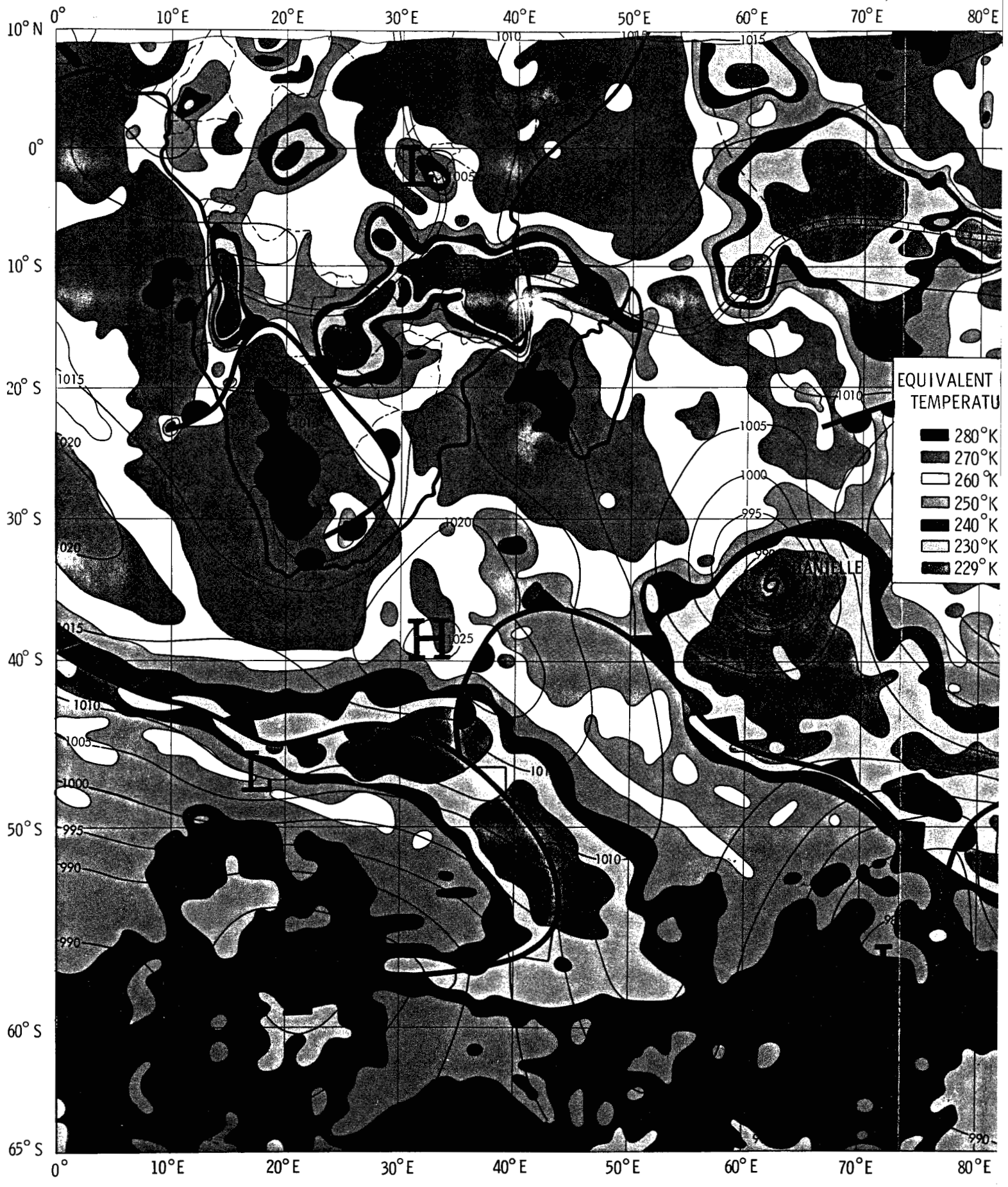

Figure 13 - Composite map of "window" radiation from TIROS VII (Channel 2) for orbits 3196-3202, on January
The surface synoptic map that is superimposed was based mainly on the South African Meteorological

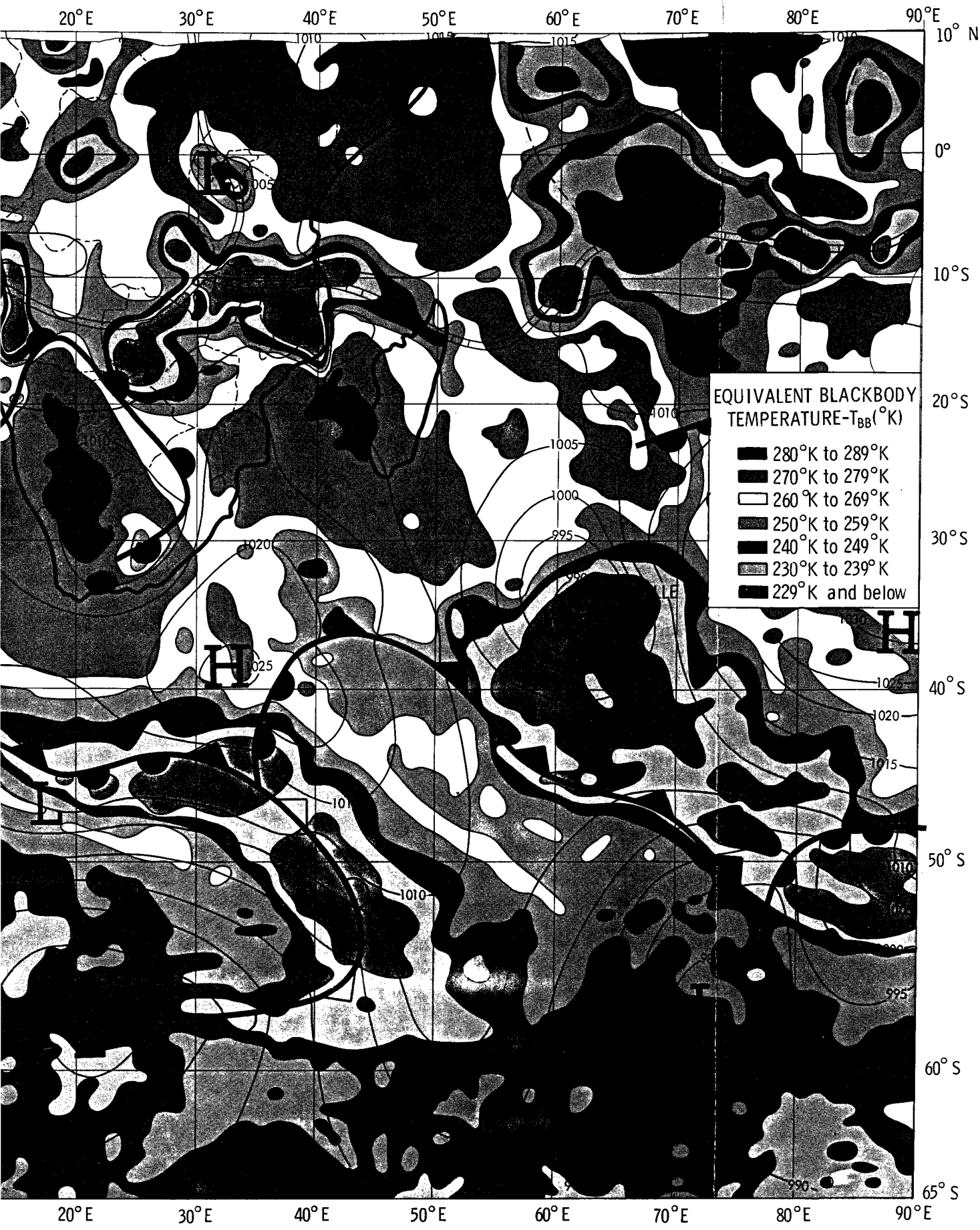

ap of "window" radiation from TIROS VII (Channel 2) for orbits 3196-3202, on January 21-22, 1964. synoptic map that is superimposed was based mainly on the South African Meteorological Office analyses.

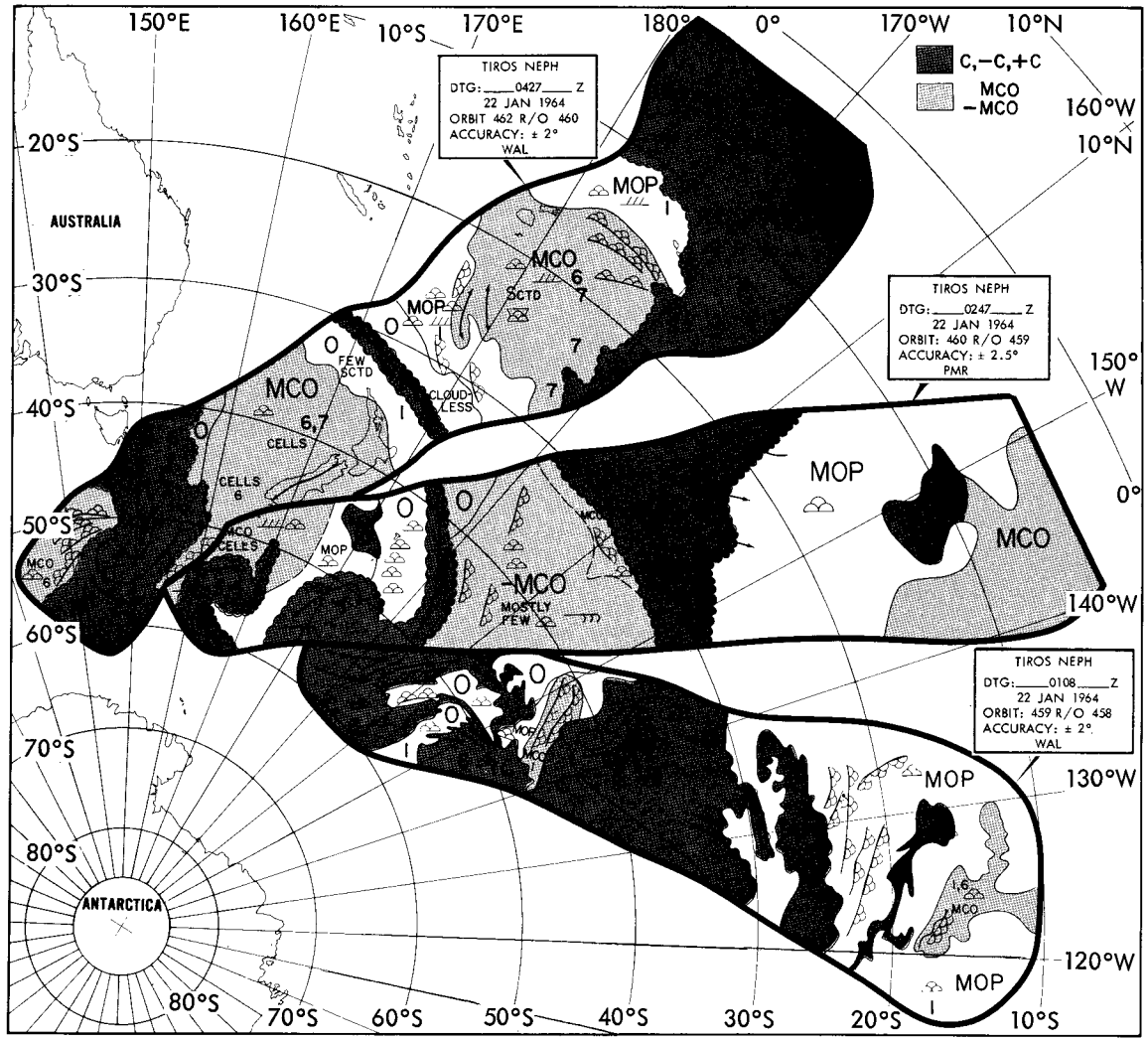

Figure 14a—Nephanalysis of TIROS VIII television pictures on January 22, 1964, in the Southern Hemisphere.

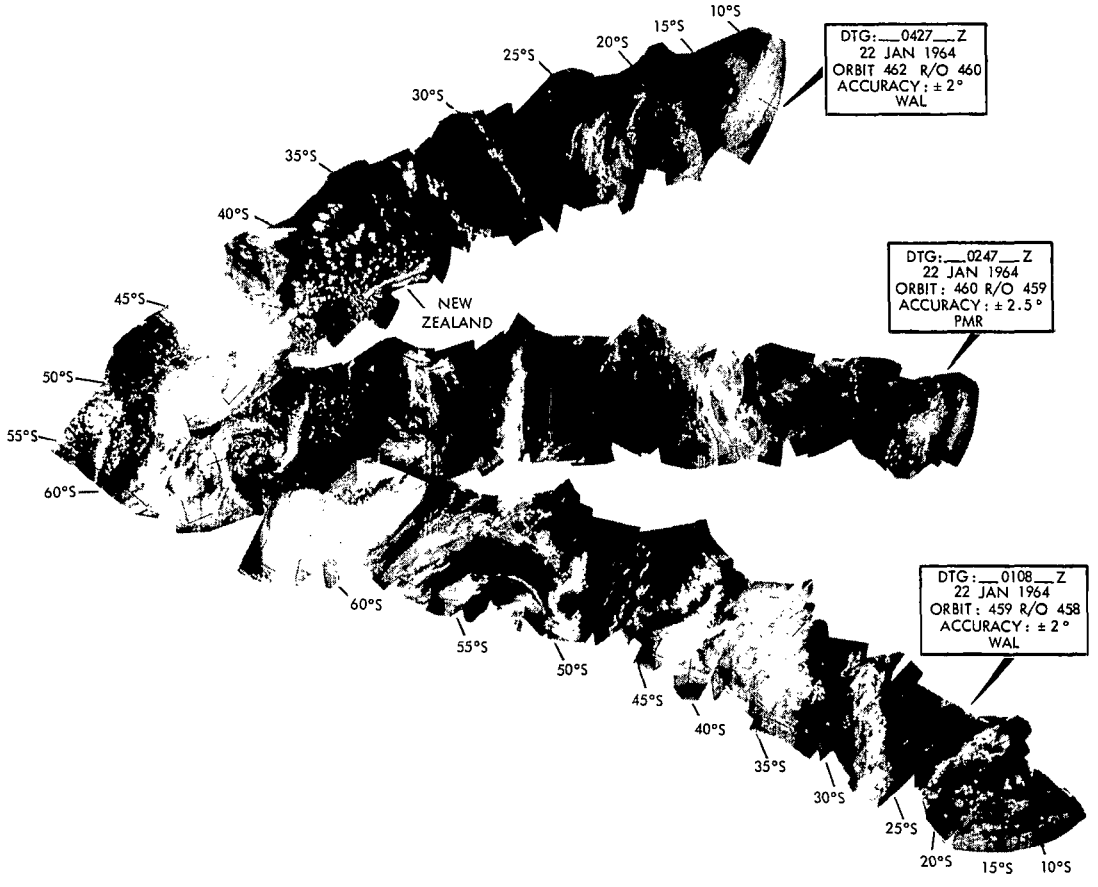

Figure 14b—Mosaic of TIROS VIII television pictures on January 22, 1964, in the Southern Hemisphere.

In the north central Australian area, the intertropical front passes through the central deserts with weak cloud activity. However, where mid-latitude frontal systems join it along the northeast coast, considerable cloudiness is suggested by the radiation measurements (Plate 1) and is supported by the surface observations. Along the southwest coast of Australia, radiation data indicate a cold front touching the Cape Leeuwin area. The television mosaic and nephanalysis (Figures 12) show these cloud patterns. The frontal system over New Zealand can be traced by radiation and television data from the Cook Strait to 55°S in the same figures.

A vertical cross-section along 10°E (Figure 15) was analyzed from the equator to 70°N for 1200 GMT January 21, 1964. Since a cross-section through a distinct squall line and frontal system was analyzed over the United States in a July 1961 study (Reference 6) this analysis was purposely drawn through an area of more complex but weaker Afro-European winter frontal activity.

In Figure 15, as in the previous analyses (References 3 and 6), the recorded "window" radiation temperatures (T_{BB}) were translated into radiation height by use of radiosonde data along the 10°E line of the cross-section (Figure 16). Ideally, the radiation height profile should follow the tops of the cloud decks and then lower to the earth's surface in clear sky regions. However, clouds do not radiate as perfect blackbodies. Cirrus clouds in particular act as if they are partially transparent and permit the warmer radiation from below to be recorded by the TIROS radiometer. Hence, the radiation heights would tend to fall below the top level of the highest cloud layers. On occasion, the sky condition may be broken to scattered and the field of view of the radiometer may not be filled completely by clouds. This may cause the radiometer to integrate energy from the earth and the clouds, and obtain an unrepresentative reading for the tops of the clouds. Compensation for atmospheric losses due to absorption of infrared energy (mainly by water vapor and ozone in the 8-12μ region) must be provided to get a correct radiation height profile. The cumulative results of these effects could cause the T_{BB} values to read 9° to 15°C lower than they should under clear sky conditions (Reference 7). In Figure 15, from 57°N to 61°N, the sky condition is a composite of scattered, broken, and overcast cloud decks at all three levels. Therefore, the radiation height could be anywhere in the lower and middle troposphere. A similar complicated cloud condition with regard to radiation height occurs farther south over the Mediterranean Sea (35°N) and in North Africa near 16°N to 18°N.

Cumulonimbus activity in the form of scattered cells is found deep inside the polar air mass over the Norwegian Sea. While low stratus clouds are associated with the small warm sector north of the German coasts, small convective clouds over the cold underlying land and water are found related to the maritime cold front over Denmark (Figure 16). Areas of variable high and low cloudiness alternate with areas of clear skies and low surface temperatures in the anticyclone over Central Europe. The warmer Mediterranean indicates more pronounced convective cloud activity but the T_{BB} values still remain about 260° to 270°K. In the north African-Sahara Desert region, the middle troposphere is dry but cirrus patches complicate the radiation height profile. Since a uniform cloud deck does not fill the field of view of the radiometer, this causes the T_{BB} values to be averaged warmer and therefore the radiation height is lower. Some allowance should also be made for the longitudinal displacement of radiosonde station data in the African region from the 10°E longitude line where the cross-sectional radiation measurements were determined.

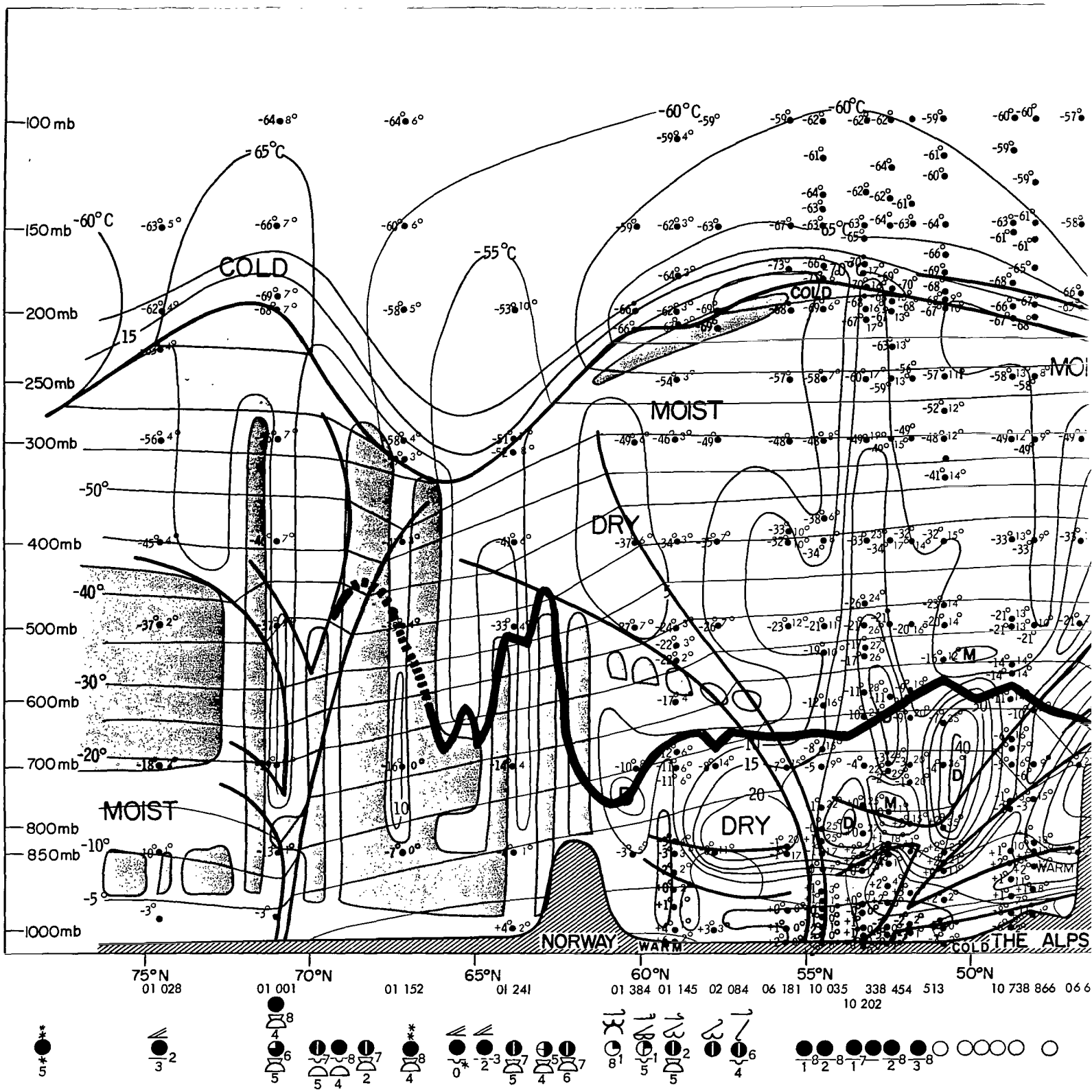
100 mb
150mb
200mb
250mb
300mb
400mb
500mb
600mb
700 mb
800mb
850mb
1000mb
-50°
-40°
-30°
-20°
-10°
-5°
-65°C
-60°C
-55°C
COLD
MOIST
DRY
MOIST
DRY
COLD
MOIST
NORWAY
WARM
COLD
THE ALPS
WARM
75°N
70°N
65°N
60°N
55°N
50°N
01 028
01 001
01 152
01 241
01 384
01 145
02 084
06 181
10 035
338 454
513
10 202
10 738
866

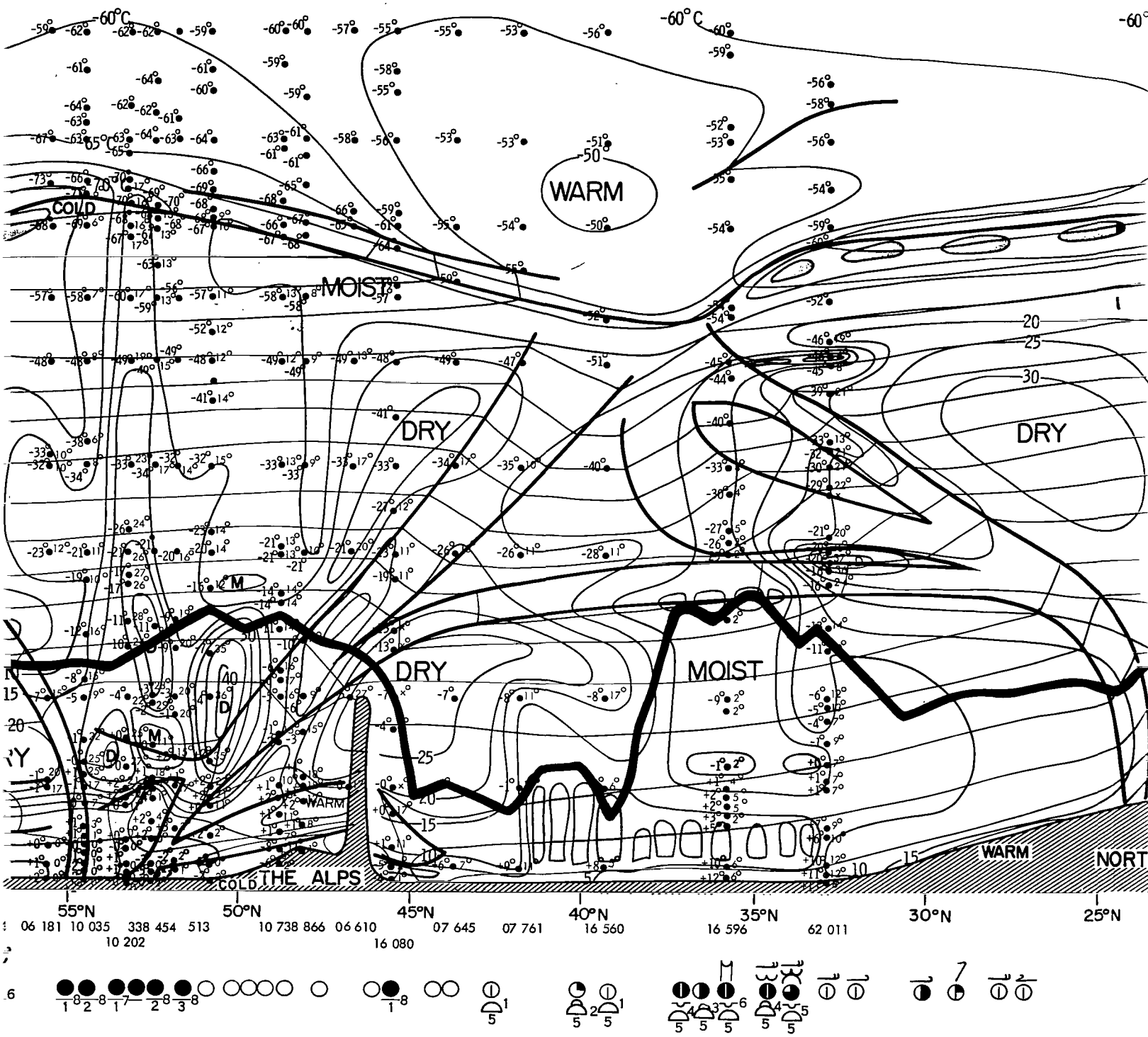

Figure 1
discontin
temperat
and also
produce
ments of
the blac

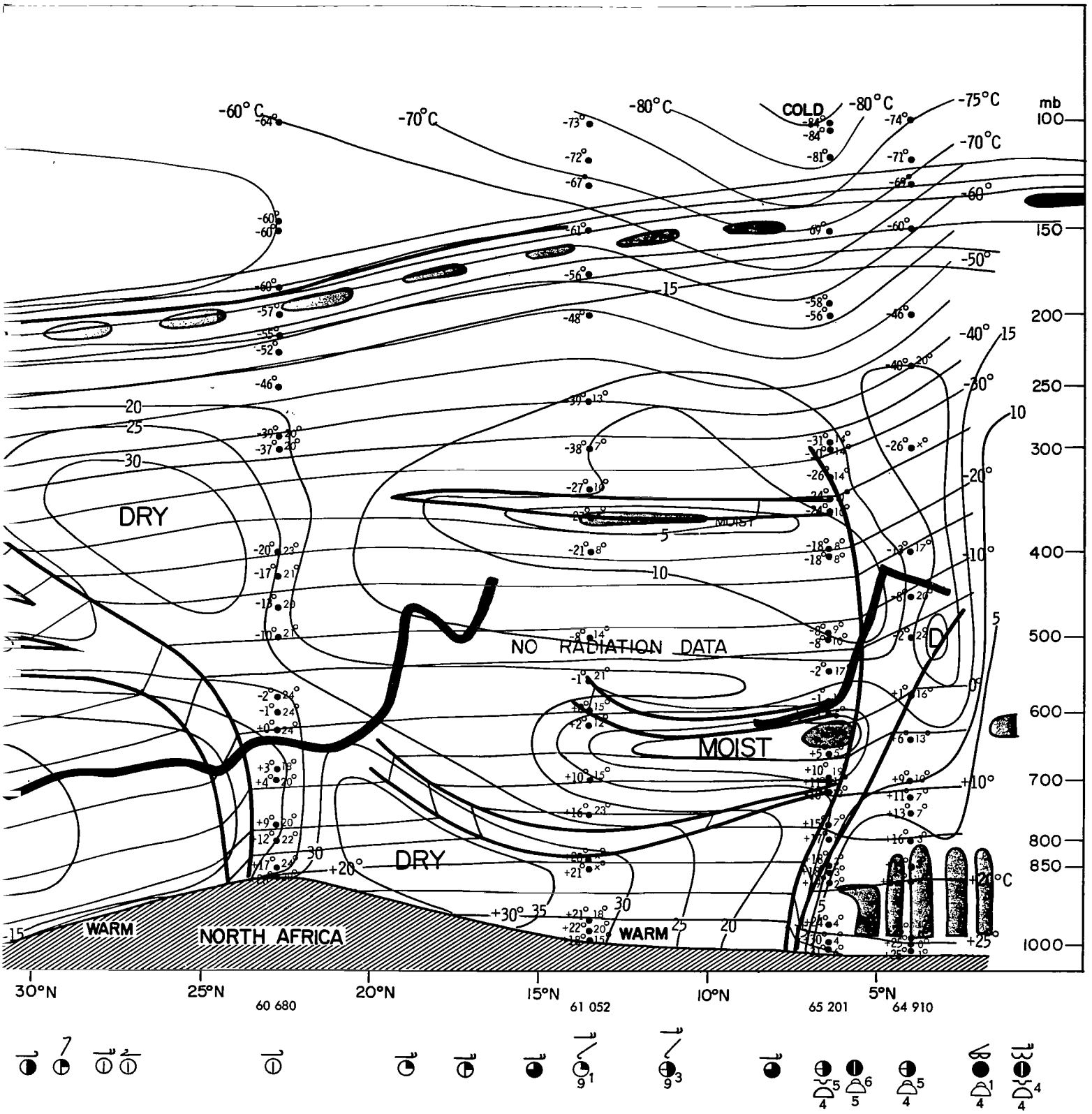

Figure 15—Vertical cross section along 10°E on 1200 GMT, 21 January 1964. Temperatures are in °C. Thermal discontinuities are indicated in a conventional manner. The humidity distribution is presented in isolines of temperature-dewpoint differences in °C. The gray shade indicates a 20°C and less temperature-dewpoint difference and also indicates schematically the cloud systems shown symbolically in the conventional surface observations reproduced at the bottom of the figure. The heavy solid line represents the effective blackbody temperature measurements of Channel 2 and conventional radiosonde data. The plotting model used shows air temperature to the left of the black dot and air temperature-dewpoint temperature difference on the right.

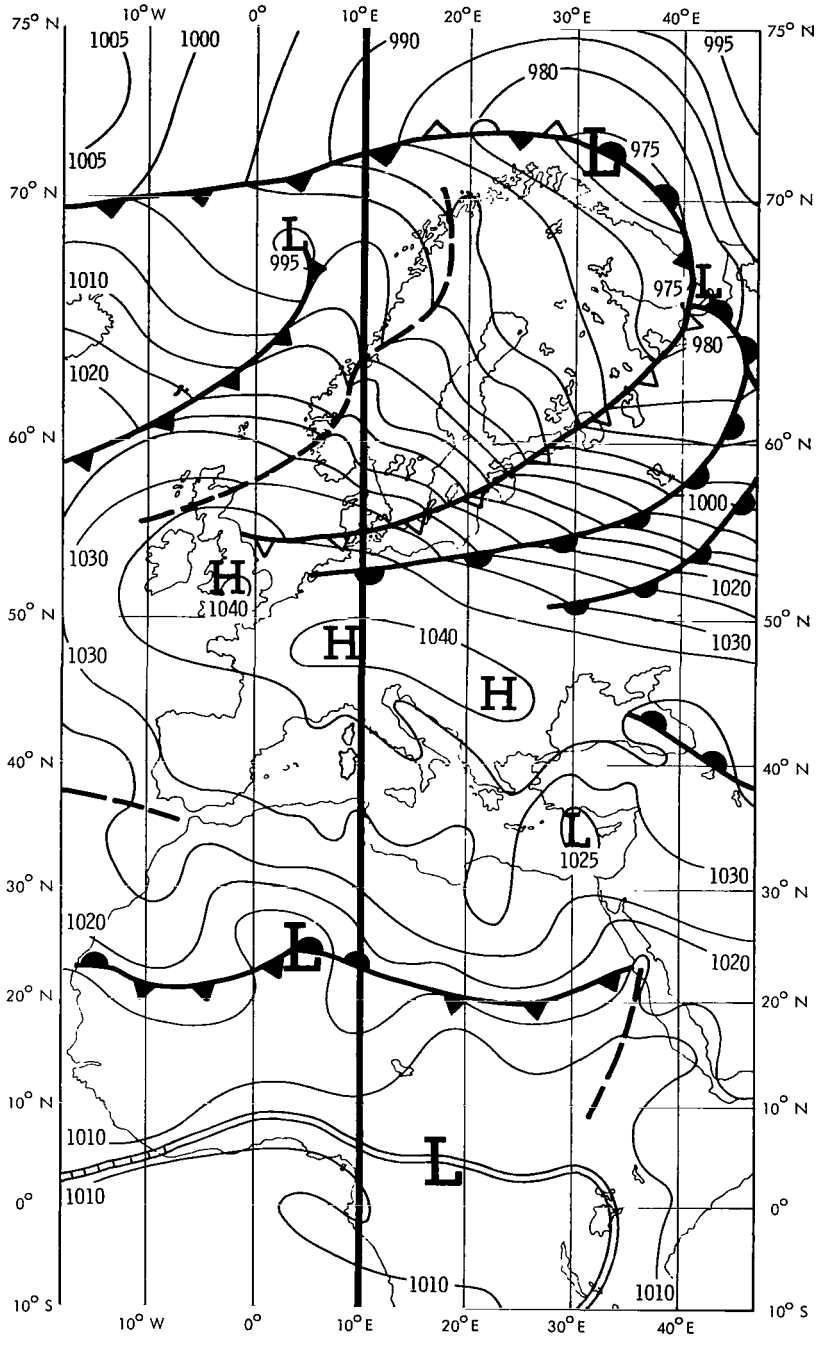

Figure 16—Surface synoptic chart at 1200 GMT, January 21, 1964 over the Afro-European area.

CONCLUSION

The patterns of outgoing radiation in the 8-12μ "window" region which were analyzed from TIROS VII and III radiation data show a good correlation with global synoptic and climatological weather information. The extension of several extratropical frontal systems into the subtropics in the southern hemisphere summer is indicated. Future satellite synoptic-radiation research should be conducted in order to determine the physical mechanism for the interaction of mid-latitude extratropical storms with the data sparse region of the intertropical zone of convergence.

ACKNOWLEDGMENTS

The authors wish to express their appreciation to the international and national meteorological services who provided the synoptic surface and upper air data used in the global weather analyses. We also wish to thank Dr. William Nordberg and Mr. William R. Bandeen of the Goddard Space Flight Center, and Mr. Thomas I. Gray, Jr., and Mr. Fred Godshall of the Environmental Science Services Administration for their contributions and suggestions.

Goddard Space Flight Center
National Aeronautics and Space Administration
Greenbelt, Maryland, September 16, 1966
160-44-04-02-51

REFERENCES

1. TIROS VII Radiation Data Catalog and Users' Manual: Volume 1, Appendix B, 19 June 1963 — 30 September 1963, Goddard Space Flight Center, September 30, 1964.
2. TIROS VII Radiation Data Catalog and Users' Manual: Volume 2, 1 October 1963 — 29 February 1964, Goddard Space Flight Center, December 31, 1964.
3. Allison, L. J., Gray, T. I., Jr., and Warnecke, G., "A Quasi-Global Presentation of TIROS III Radiation Data," NASA SP-53, 1964.
4. Bandeen, W. R., Halev, M., and Strange, I., "A Radiation Climatology in the Visible and Infrared from the TIROS Meteorological Satellites," NASA TN D-2534, June 1965.
5. Weickmann, L., "Mittlere Luftdruckverhaeltnisse im Meeresniveau waehrend der Hauptjahreszeiten im Bereiche um Afrika, in dem Indischen Ozean und den angrenzenden Teilen Asiens," Meteorologische Rundschau, 16 Jahrg., Heft 4, pp. 89-100, 1963.
6. Allison, L. J., and Warnecke, G., "The Interpretation of TIROS Radiation Data for Practical Use in Synoptic Weather Analysis," NASA TN D-2851, June 1965.
7. Greaves, J. R., Wexler, R., and Bowley, C. J., "The Feasibility of Sea Surface Temperature Determination Using Satellite Infrared Data," Final Report, 9G16-F, Aracon Geophysics, Co., Concord, Mass., Nov. 1965, 47 pp.

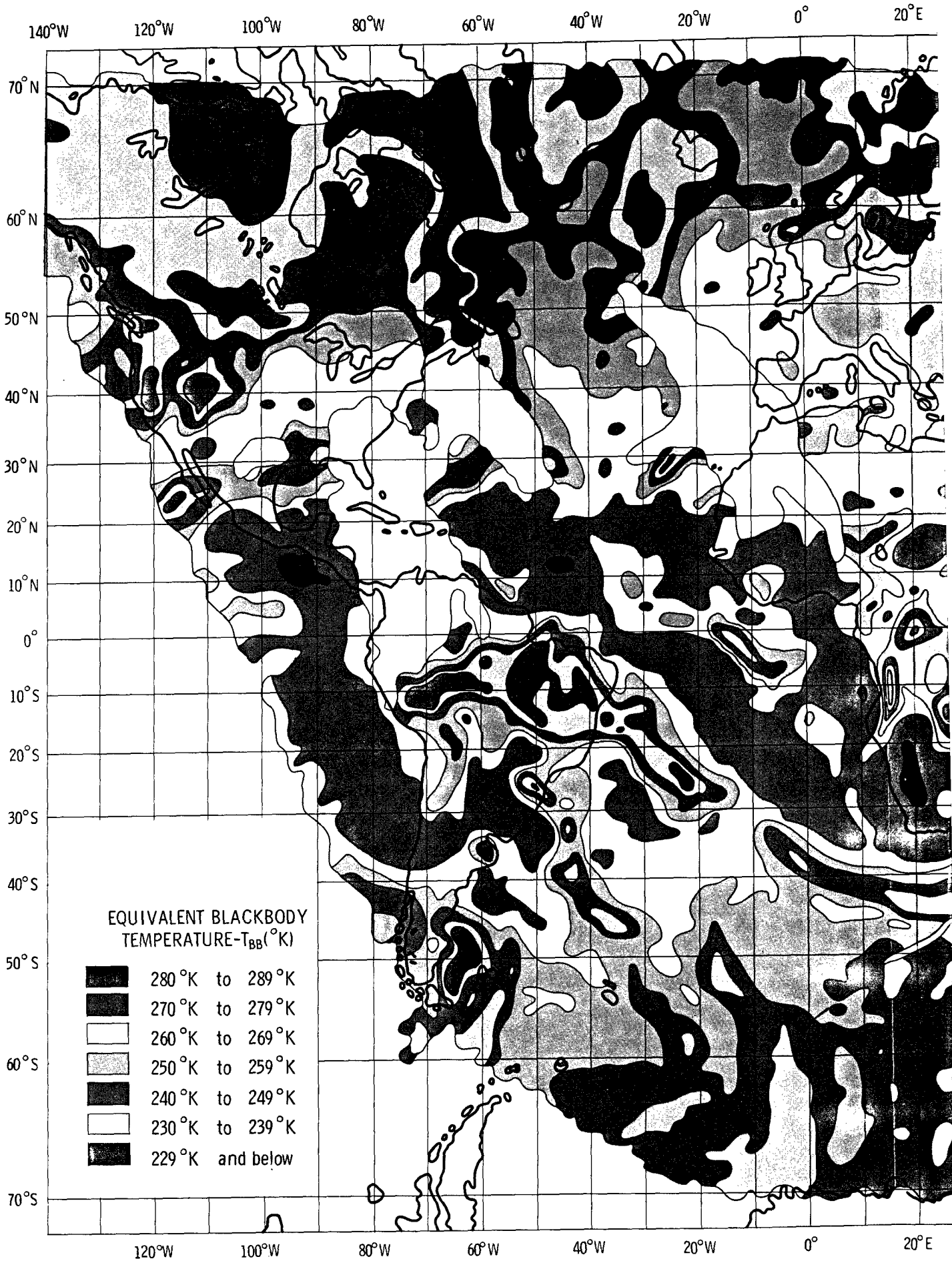
140°W
120°W
100°W
80°W
60°W
40°W
20°W
0°
20°E
70°N
60°N
50°N
40°N
30°N
20°N
10°N
0°
10°S
20°S
30°S
40°S
50°S
60°S
70°S
EQUIVALENT BLACKBODY TEMPERATURE-T_{BB}(°K)
280 °K to 289 °K
270 °K to 279 °K
260 °K to 269 °K
250 °K to 259 °K
240 °K to 249 °K
230 °K to 239 °K
229 °K and below

Plate

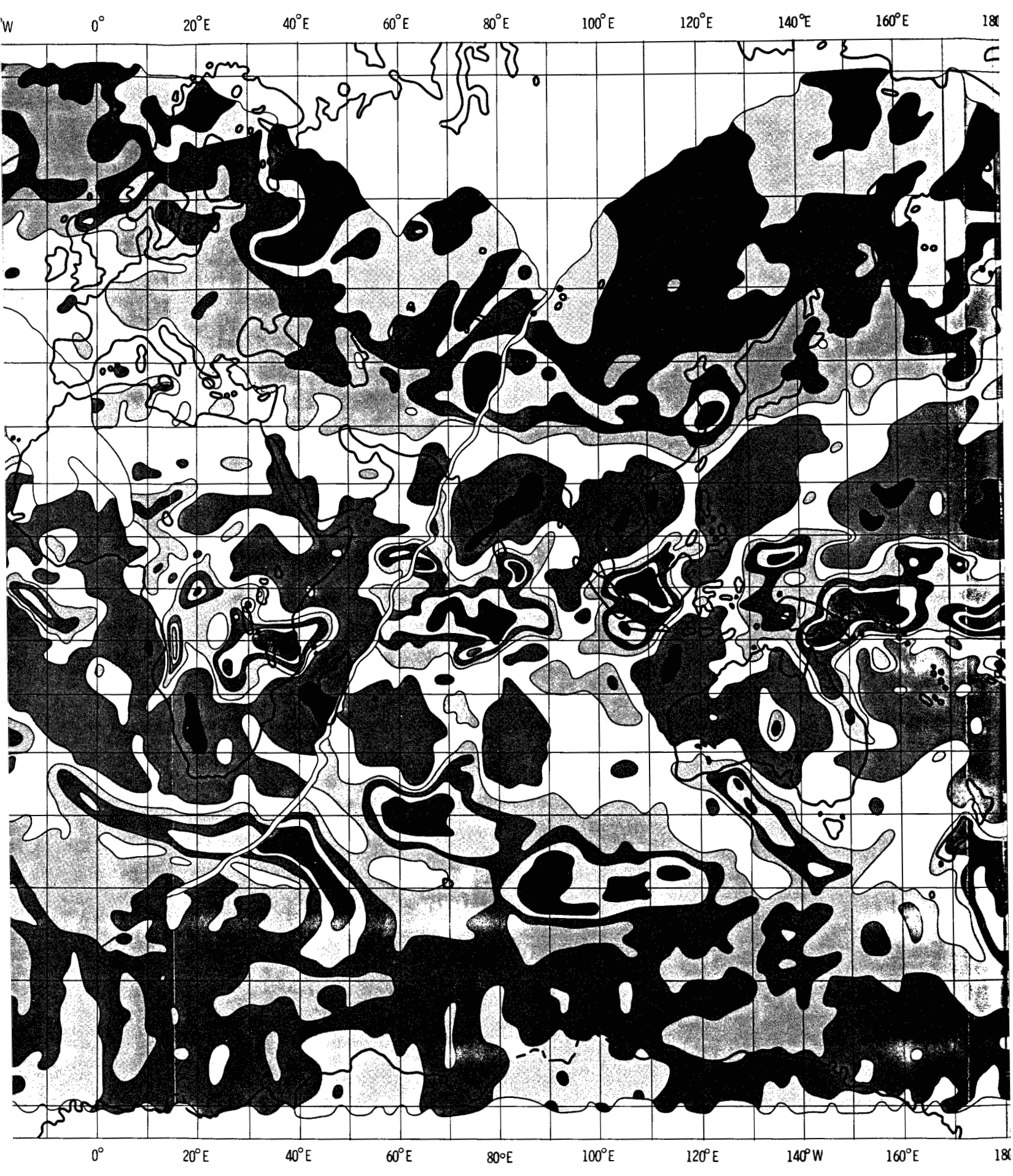

Plate 1 - Composite map of "window" radiation from TIROS VII (Channel 2) for orbits 3195-3203; on January 21-22, 1964.

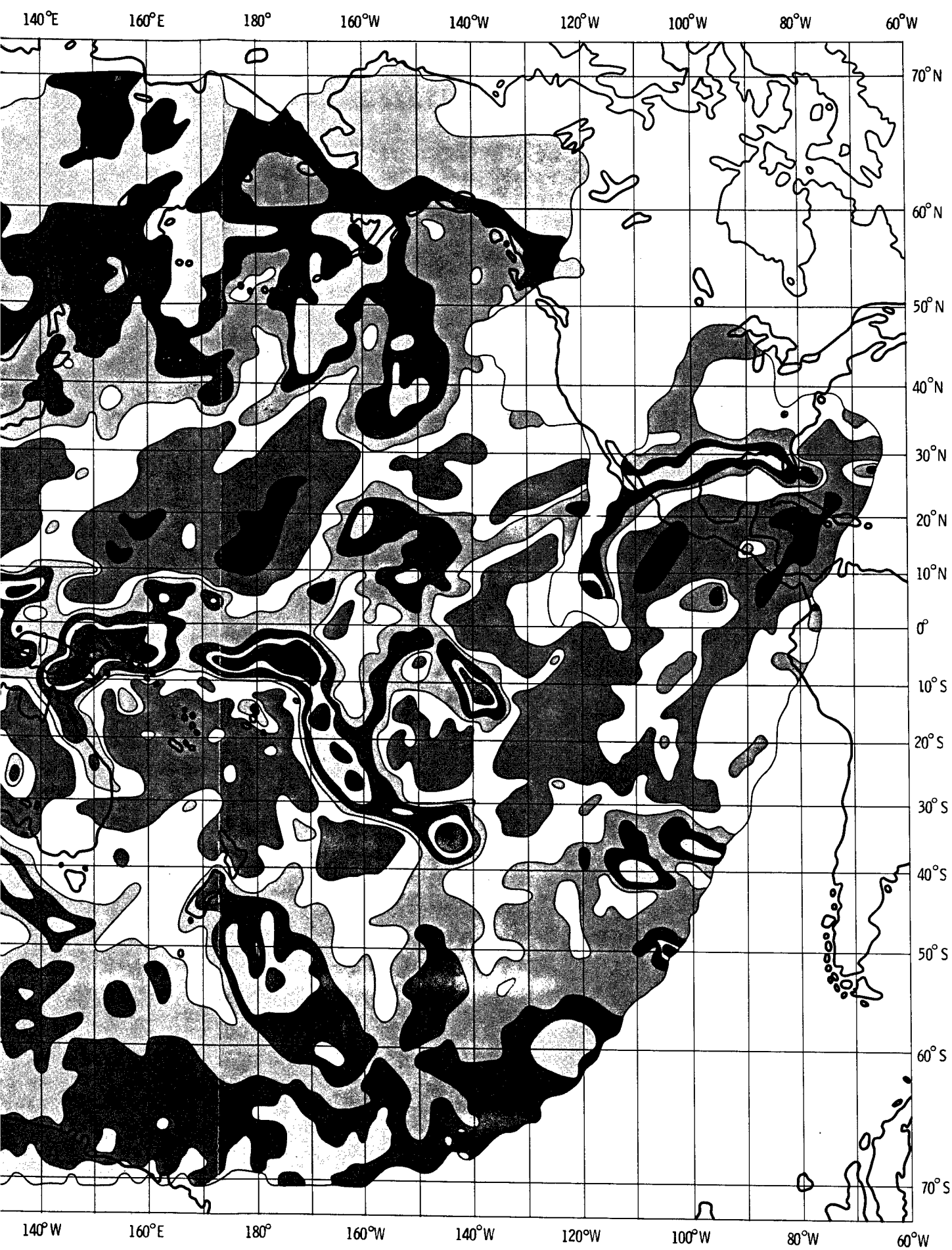
140°E
160°E
180°
160°W
140°W
120°W
100°W
80°W
60°W
70°N
60°N
50°N
40°N
30°N
20°N
10°N
0°
10°S
20°S
30°S
40°S
50°S
60°S
70°S
140°W
160°E
180°
160°W
140°W
120°W
100°W
80°W
60°W

annel 2)
1964.

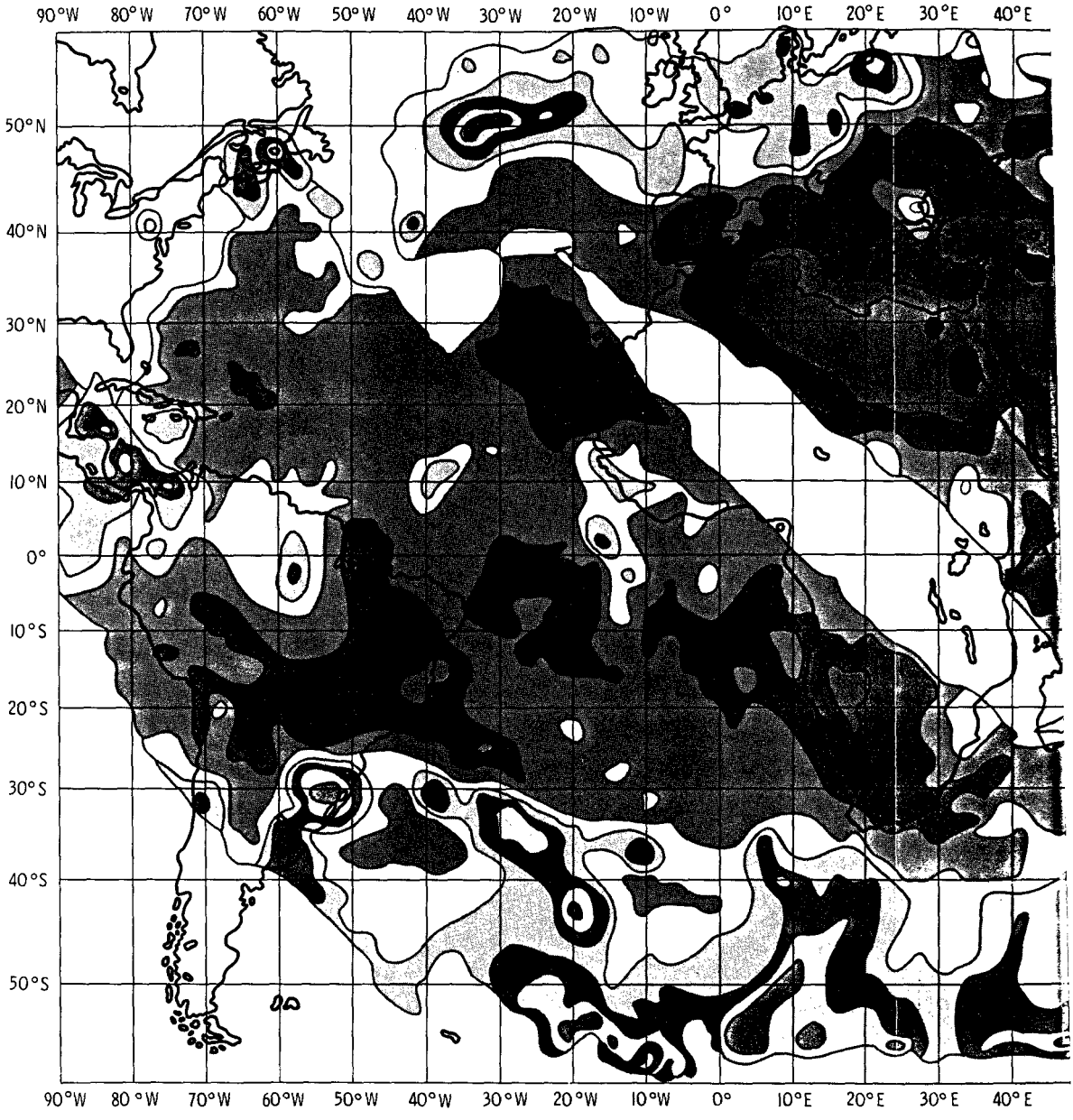
90°W 80°W 70°W 60°W 50°W 40°W 30°W 20°W 10°W 0° 10°E 20°E 30°E 40°E
50°N
40°N
30°N
20°N
10°N
0°
10°S
20°S
30°S
40°S
50°S
90°W 80°W 70°W 60°W 50°W 40°W 30°W 20°W 10°W 0° 10°E 20°E 30°E 40°E

F

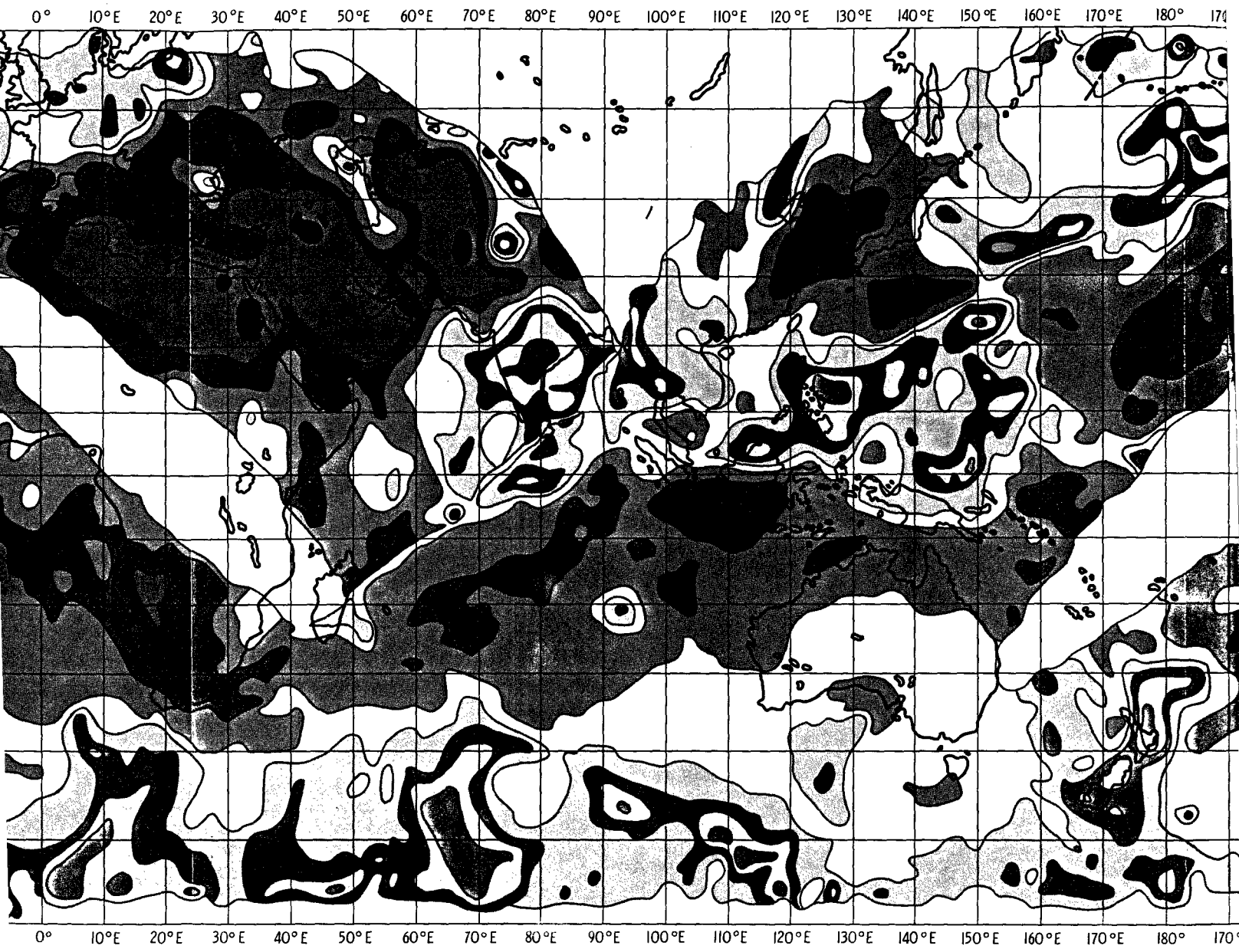

Plate 2 - Composite map of "window" radiation from TIROS III (Channel 2) for orbits 56, 57, 58, 60 through 63, on July 16, 1961.

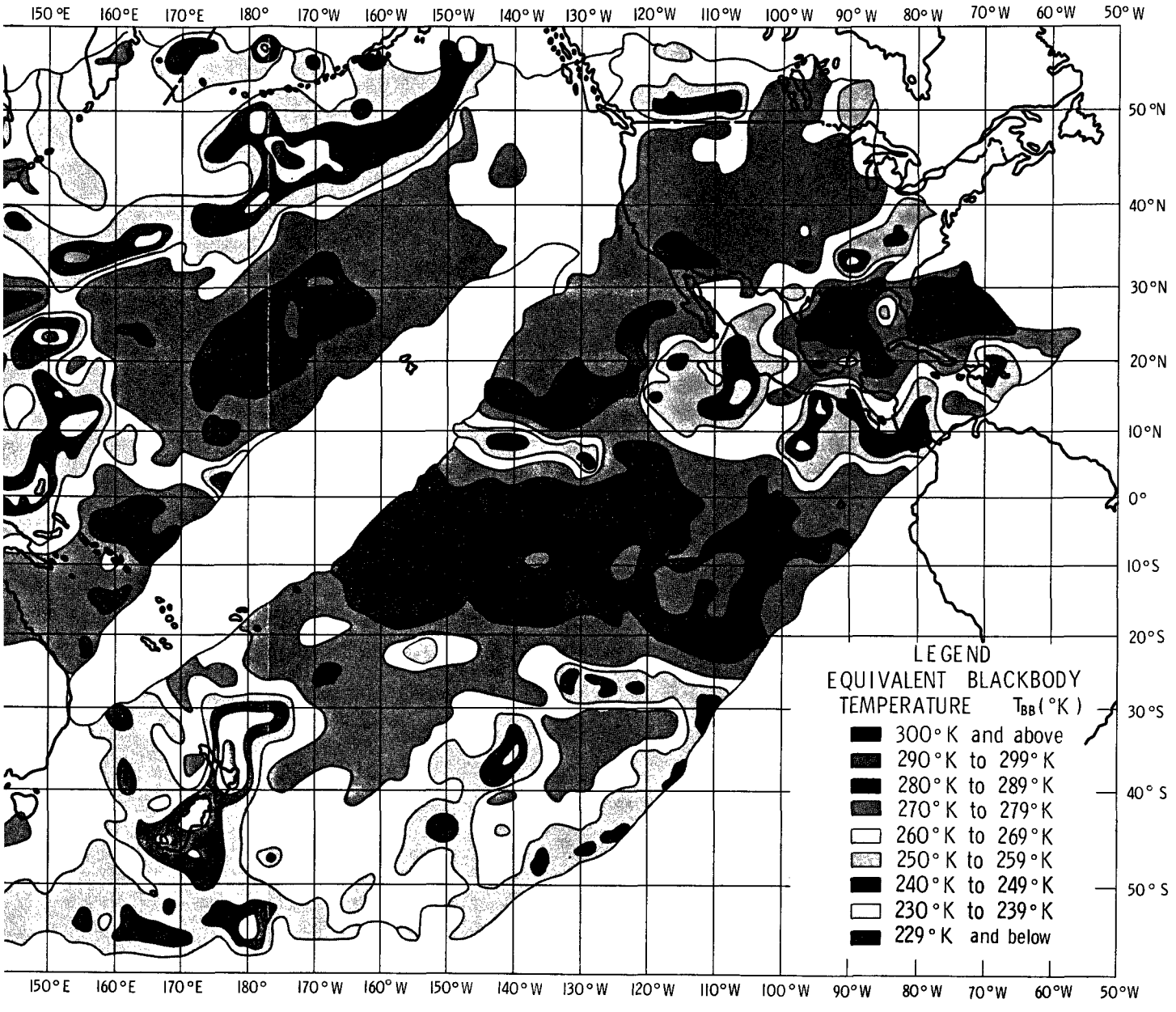

ROS III (Channel 2)
, on July 16, 1961.

"The aeronautical and space activities of the United States shall be conducted so as to contribute . . . to the expansion of human knowledge of phenomena in the atmosphere and space. The Administration shall provide for the widest practicable and appropriate dissemination of information concerning its activities and the results thereof."

—NATIONAL AERONAUTICS AND SPACE ACT OF 1958

NASA SCIENTIFIC AND TECHNICAL PUBLICATIONS

TECHNICAL REPORTS: Scientific and technical information considered important, complete, and a lasting contribution to existing knowledge.

TECHNICAL NOTES: Information less broad in scope but nevertheless of importance as a contribution to existing knowledge.

TECHNICAL MEMORANDUMS: Information receiving limited distribution because of preliminary data, security classification, or other reasons.

CONTRACTOR REPORTS: Scientific and technical information generated under a NASA contract or grant and considered an important contribution to existing knowledge.

TECHNICAL TRANSLATIONS: Information published in a foreign language considered to merit NASA distribution in English.

SPECIAL PUBLICATIONS: Information derived from or of value to NASA activities. Publications include conference proceedings, monographs, data compilations, handbooks, sourcebooks, and special bibliographies.

TECHNOLOGY UTILIZATION PUBLICATIONS: Information on technology used by NASA that may be of particular interest in commercial and other non-aerospace applications. Publications include Tech Briefs, Technology Utilization Reports and Notes, and Technology Surveys.

Details on the availability of these publications may be obtained from:

SCIENTIFIC AND TECHNICAL INFORMATION DIVISION

NATIONAL AERONAUTICS AND SPACE ADMINISTRATION

Washington, D.C. 20546